17.2.4 Collaboration for SDG best practice

SRI KRISHNA COLLEGE OF ENGINEERING AND TECHNOLOGY
An Autonomous Institution| Approved by AICTE| Affiliated to Anna University
Kuniamuthur, Coimbatore – 641008
Phone: (0422)-2628001 (7 Lines) | Email : info@skcet.ac.in | Website: www.skcet.ac.in

List of International Events

S.No	Name of the University/ Organization	International faculty in contact with details	Date of Interaction	Event Name	SDG
1.	Connected Computing and Media Processing Lab, Kyungpook National University South Korea	Dr. Anand Paul Director	04.08.2022	University Collaborations - Conference, Webinar, Seminar, Paper Publications	4,7,9
2.	Microsoft, Seattle,USA	Mr. R. Dhanasekaran Principal Product Manager	19.04.2023	Webinar on Product Management and its Financials in Microsoft	12
3.	International Lecture Series on Academic Research - An Insight for the Civil Engineering Faculty and Students	Prof. Ir. Dr. Ubagaram Johnson Alengaram, Centre for Innovative Construction Technology, Department of Civil Engineering	02.03.2023	International Keynote address on International Lecture Series on Academic Research - An Insight for the Civil Engineering Faculty and Students	4,7,9
4.	Akka Technologies Germany.	Mr.Muthiah, Computation Engineer,	14.10.2022	International Conference on Innovations in Robotics, Intelligent Automation and Control (ICIRIAC 2022)	4
5.	Apple Inc., California, USA.	Mr. Laxman Subramanian Global Sourcing Manager	15.9.2022	Workshop on Industrial IOT & Automation	4,8
6.	Technical University	Dr. Andreas Rau,	30.08.2022	Guest Lecture on Transport Demand	11

	of Munich Asia, Singapore	Faculty Head and Principal Investigator (Rail, Transport and Logistics)		Management	11
7.	Connected Computing and Media Processing Lab, Kyungpook National University	Dr. Anand Paul Director	04.08.2022	State space Navigation for Intelligent Robotic Agents	4,9

MECHATRONICS ENGINEERING ASSOCIATION

14.10.2022	**International Conference on Innovations in Robotics, Intelligent Automation and Control (ICIRIAC 2022)**	➢ **Dr. Anand Paul, Director, Connected Computing and Media Processing Lab, Kyunpook National University. South Korea.** ➢ **Mr.Muthiah, Computation Engineer,Akka Technologies,Germany.**

Photography Highlights of the event:

SRI KRISHNA COLLEGE OF ENGINEERING AND TECHNOLOGY

An Autonomous Institution| Approved by AICTE| Affiliated to Anna University
Kuniamuthur, Coimbatore - 641008

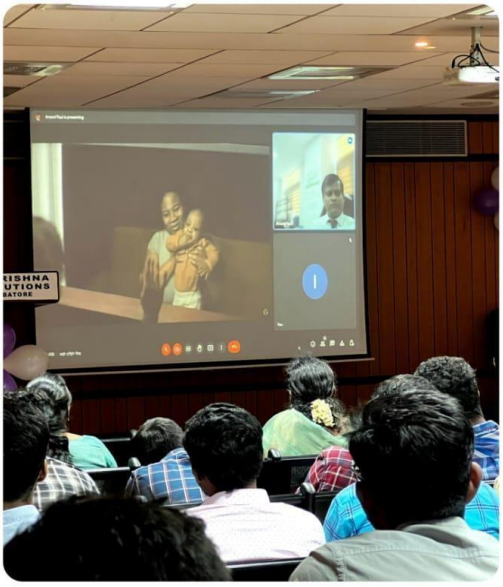

SRI KRISHNA COLLEGE OF ENGINEERING AND TECHNOLOGY

An Autonomous Institution| Approved by AICTE| Affiliated to Anna University

Kuniamuthur, Coimbatore - 641008

SRI KRISHNA COLLEGE OF ENGINEERING AND TECHNOLOGY

Kuniamuthur, Coimbatore. Tamil Nadu 641008

(An Autonomous Institution Affiliated to Anna University, Chennai)

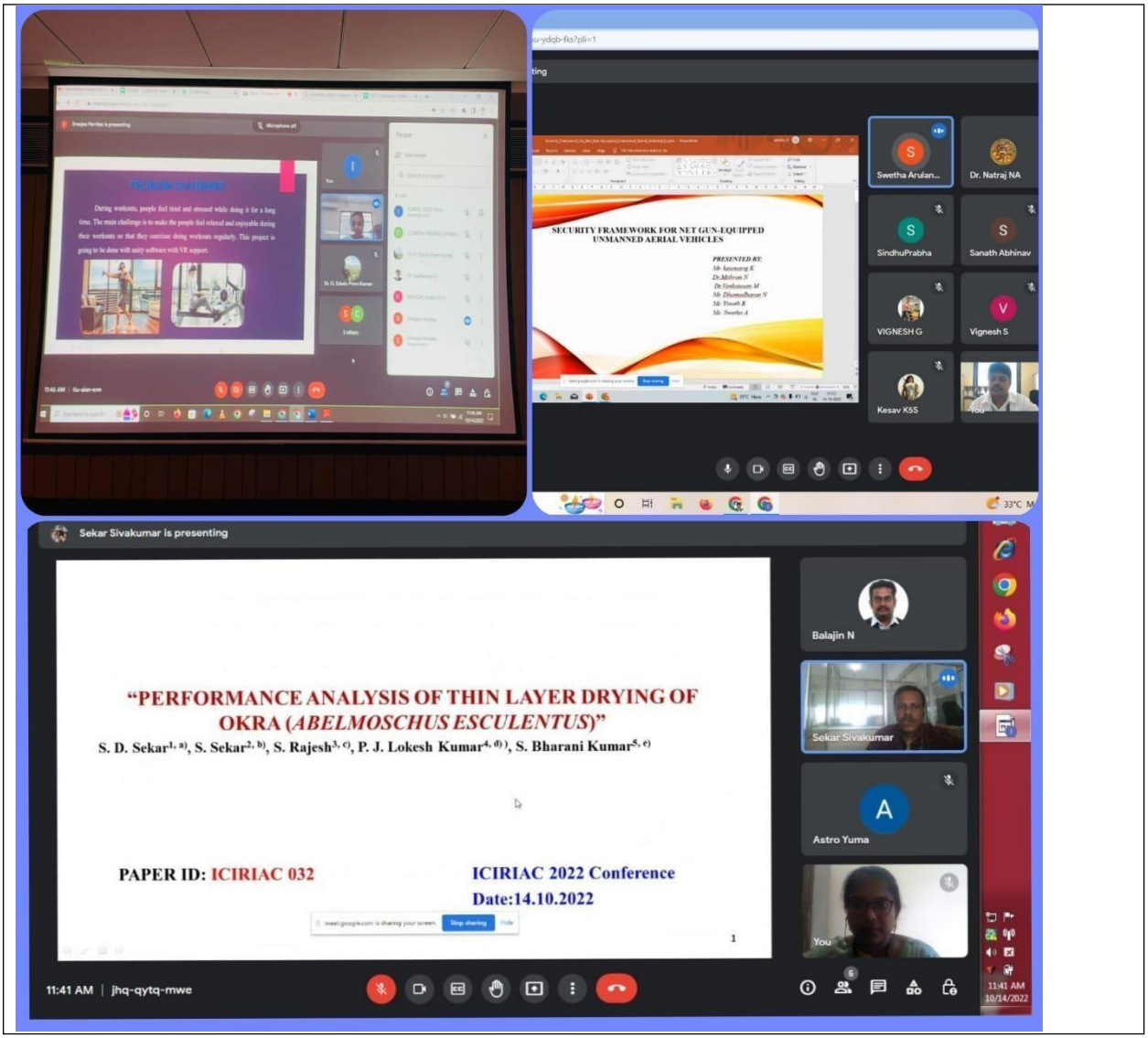

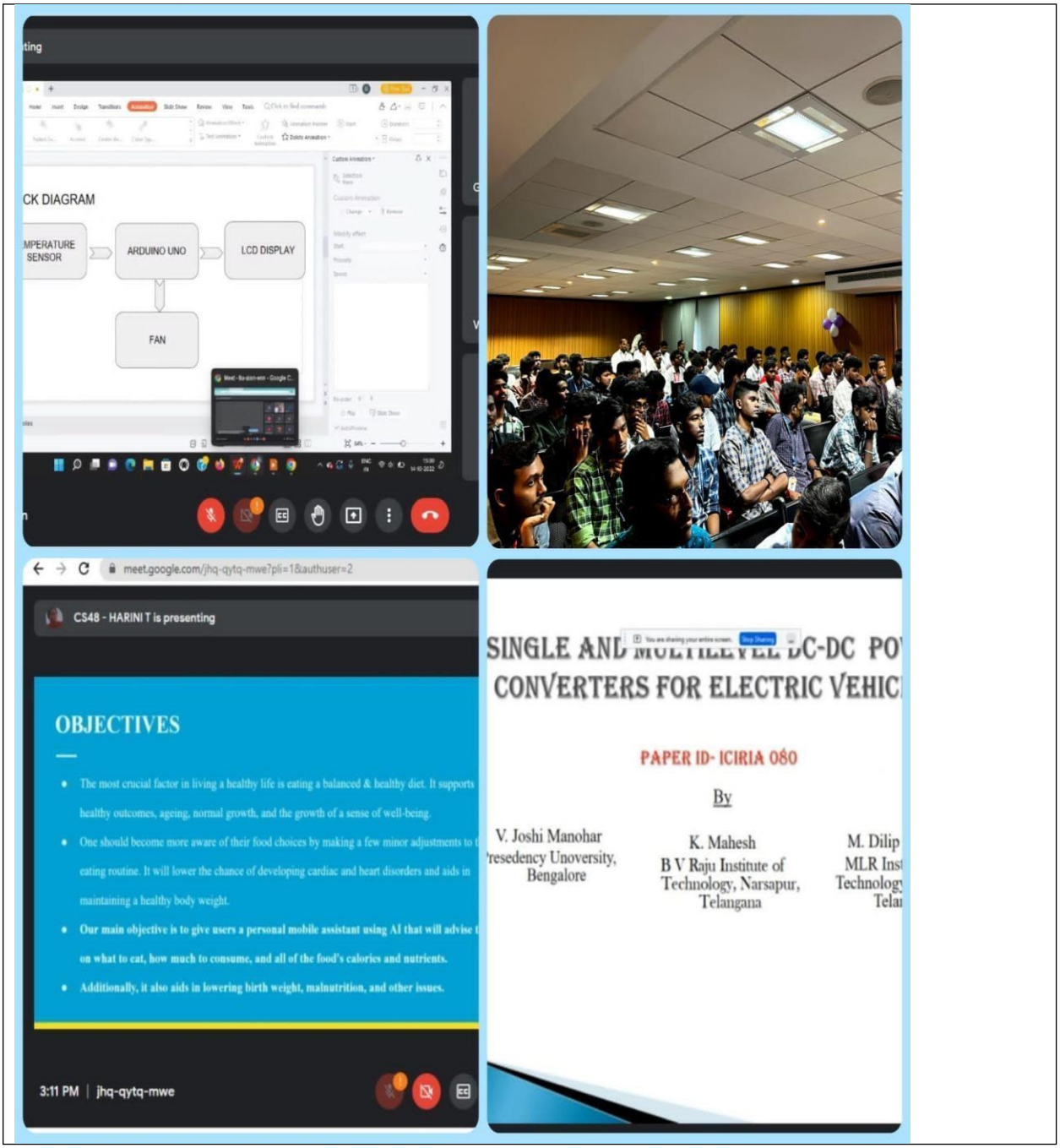
CK DIAGRAM
MPERATURE SENSOR
ARDUINO UNO
LCD DISPLAY
FAN
meet.google.com/jhq-qytq-mwe?pli=1&authuser=2
CS48 - HARINI T is presenting
OBJECTIVES
The most crucial factor in living a healthy life is eating a balanced & healthy diet. It supports healthy outcomes, ageing, normal growth, and the growth of a sense of well-being.
One should become more aware of their food choices by making a few minor adjustments to t eating routine. It will lower the chance of developing cardiac and heart disorders and aids in maintaining a healthy body weight.
Our main objective is to give users a personal mobile assistant using AI that will advise t on what to eat, how much to consume, and all of the food's calories and nutrients.
Additionally, it also aids in lowering birth weight, malnutrition, and other issues.
3:11 PM | jhq-qytq-mwe
CONVERTERS FOR ELECTRIC VEHIC
PAPER ID- ICIRIA 080
By
V. Joshi Manohar
resedency Unoversity, Bengalore
K. Mahesh
B V Raju Institute of Technology, Narsapur, Telangana
M. Dilip
MLR Inst Technology Telan

Department of Mechatronics Engineering in association with Kyunpook National University, South korea organized International Conference on Innovations in Robotics, Intelligent Automation and Control (ICIRIAC 2022). 2 keynote addresses and 6 Technical sessions were organized in this conference. The Best Papers Awards were announced and appreciated.The organizing committee members, Chairs, Co-chairs, student volunteers were appreciatedwith certificates.

List of participants

Manuscript Addressing SDG 1 to 17

S.NO	Paper ID	Title of the Article	Authors Name
1	ICIRIAC 003	Analyzing and Securing Information, Images of Women in Online portal using CNN algorithm	Ganesh D R, Chithambarathanu M
2	ICIRIAC 006	IoT Based Smart Parking System	V.Kiruthika, M.Jagadeeswari , C.Sneha Prabha, H.Sreejaa
3	ICIRIAC 007	Stress-Free Workouts Using Virtual Reality	V.Kiruthika, M.Jagadeeswari , C.Sneha Prabha, H.Sreejaa
4	ICIRIAC 009	Tomato Leaves Disease Identification by Deep Convolution Neural Network Using Inception V3	Devi.D, Prasanna N, Prateek ram RA S, Niyaz mohamed N
5	ICIRIAC 011	Ordering Program Elements According to Testing Requirements	Animesh Srivastava and Parveen Kumar Saini
6	ICIRIAC 012	Braille Board Actuates Text into Braille code using Solenoid Actuator	Vignesh T, Barath V, Barath B, Bharath K A, Bhrugunandhana K
7	ICIRIAC 013	Importance of Machine Learning in Market Research	Prashast Singh and Bhuvanesh Kumar Sharma
8	ICIRIAC 014	Guerilla Marketing and Marketing Innovations in Industry 4.0	Samarth Singh Tyagi and Mahima Mishra
9	ICIRIAC 015	Leveraging Artificial Intelligence in Enhancing Financial Inclusion for the Un-Banked and Under-Banked in India	Aashna Karmacharya, and Santosh Gopalkrishnan
10	ICIRIAC 016	Marketing automation for digital transformation: a review	Bharti Sinha and Kanchan Patil
11	ICIRIAC 017	Virtual Reality in Sports – Redefining Audience Engagement and Expectations	Piyasha Sarkar and Mun Mun Ghosh
12	ICIRIAC 018	Impact of Local Cultures on Implementation of Industry 4.0	Mahesh Shinde, Naim Shaikh, Kishori Kasat
13	ICIRIAC 019	Conceptual Framework for Adaptive Access and Identity Management	Savio Extros and Nisha TN
14	ICIRIAC 020	The Need for Marketing Automation: A Review	Attideep Raina, and Hemraj Lamkuche

15	ICIRIAC 021	Automation, Technological Employment, And Society	Ritesh Khatwani, Gopala Raghuram and Mahima Mishra
16	ICIRIAC 022	Impact of Virtual Reality on Consumer Buying Behaviour in India	Trisha Singh, Atish Ratan Dasgupta and Semila Fernandes
17	ICIRIAC 023	The Study of Evolution of Artificial Neural Network Systems and Development of Computational Intelligent Systems Using Artificial Intelligence for Improving the Performance in Financial Markets	Madhura Ranade, Aniruddha Joshi and Lavi Gupta
18	ICIRIAC 024	Application of Modern AR/VR Technologies in Brand Promotion	Himanshu Singh and Prasanna Kulkarni
19	ICIRIAC 025	Success Factors for Chat bots from the Perspective of an Indian Customer	Deven Bhalerao, Shaji Joseph
20	ICIRIAC 026	Impact of Automation on Productivity and Organizational Restructuring	Rajshree Sen, Vinita Sinha
21	ICIRIAC 027	Cyber Forensics in Curtailing the Growth of Cybercrimes: A Bibliographic Study	Soumya Singh and Pradnya Purandare
22	ICIRIAC 028	Competition in the RPA Industry: A Case Study of Blue Prism	Laxmikant Rane, Giri Gundu Hallur
23	ICIRIAC 029	Design and Fabrication of Smart Electric Bike	M. Vigneshwaran, A. Neelash Kannan, S. Adhithyan, S. Gopi Krishna, KP Hariharan, L. Gurunathan
24	ICIRIAC 030	Design and Fabrication of Autonomous Robot for Crop Yield Prediction and Analysis Using Machine Learning Algorithms	T.Sivaranjani, Dr.S.P.Vimal, Dr.J.Indirapriyadharshini, R.Gokila
25	ICIRIAC 031	A Highly Improved Distortion Minimizing Technique for Watermarking Relational Databases	Kavya.S.P, Prabu.K, Madesh Kumar.A, Muthu Logesh.M, Raghupathi natha Krishnan
26	ICIRIAC 032	Performance Analysis of Thin Layer Drying of Okra (Abelmoschus Esculentus)	S. D. Sekar, S. Sekar, S. Rajesh, P. J. Lokesh Kumar
27	ICIRIAC 035	Multibit Soft Error Resilient SRAM Based TCAM for FPGA	Celina Grace P and Dr S Sophia
28	ICIRIAC 038	A comparative study in predictive analytic frameworks in big data	Dr. Sudharson D, Dr.K.Vignesh, Dr.B.Suganthi, Dr. Arunkumar B, Ms. Shreya Vijay, Ms. Logita.S
29	ICIRIAC 040	A Novel Approach of Detection and Control of the Heavy Metals	Ms. Vanitha U, Hari Shruthi TK, Hemalatha A, Jothilakshmi M

		in Marine Foods Using Machine Learning	
30	ICIRIAC 041	Semi-Active Suspension Control using P-LQR method	Muthiah Shanmugam, Eric Demeester, Tegoeh Tjahjowidodo
31	ICIRIAC 042	Optimal Resource Allocation in Wireless Systems	Pavithra D and Mrs.Kalaivani
32	ICIRIAC 043	Handover policies in wireless communication systems based on MDP	Mothesvar N M and Dr V Nandalal
33	ICIRIAC 045	Diagnosis of Liver Failure using Flask Web Framework	Amruthamathi and Devi D
34	ICIRIAC 047	Detection of Sludge in Critical Region of Oil Transportation Pipelines using Robot	P. Duraimurugan, S. Rajesh, G. Mahendran, R. L. Sankarlal, V. Senthil, N. Velmurugan
35	ICIRIAC 048	MSI REGENERATION USING ENHANCED VAE-GAN	Vanitha U, Subash Niranjan B C, Hariharasudhan S, Rajkumaraah B G, Yogesh M
36	ICIRIAC 049	PERFORMANCE STUDY ON DRAFT TUBE IN KAPLAN TURBINE	Sathish K , Sabareswaran K , Balakumar B S , Bharathram B
37	ICIRIAC 050	Automated Sand Depositing System for Sand Casting	Ananthi K, Sivamani S, Priyadharsini S
38	ICIRIAC 051	STROKE PREDICTION USING ML AND IOT BASED WEARABLE DEVICE	G.Kanagaraj, T.Primya, M.Prabhavathy, P.Saranya, V.Senthilkumar
39	ICIRIAC 052	SMART SYSTEM FOR WOMEN SAFETY IN CYBERSPACE BY FAKE PROFILE DETECTION	Nandala V, Anand Kumar V, Sujitha A, Sumitha G, Sureka A S
40	ICIRIAC 054	An Effective POS-CNN-Based Adaptive Model for Classifying Brain Tumour from MRI Images	Sajeev Ram Arumugam, Thanga Mariappan L, K Makanyadevi, R Balakrishna, Sankar Ganesh Karuppasamy
41	ICIRIAC 055	Deep learning technique for prediction of covid 19 using CT images	Vanitha U, Dr. Albert Raj A, Kavya T, Khaashwini M S, Meena A
42	ICIRIAC 059	k-mer Based Prediction of Gene Family by applying Multinomial Naïve Bayes Algorithm in DNA sequence	J A M Rexie, Kumudha Raimond, Brindha D, A Kethsy Prabavathy
43	ICIRIAC 061	A SURVEY ON DESIGN AND OPTIMIZATION OF METALLIC BIOMATERIAL FOR ORTHOPAEDIC APPLICATION	Gowtham S, Dharanidharan M, Manoj S, Balakumar B S, Bharathram B

44	ICIRIAC 062	REGENERATIVE SUSPENSION SYSTEM USING LINEAR MAGNET SYSTEM	Gowtham S, Barath G, Sudharsan K, Thiyagarajan V, Balasubramani S
45	ICIRIAC 064	A review on CFD analysis of Evaporative cooling in condenser	Naveenprabhu V, Dinesh Gowtham K, Manikanda Prabu P L, Vigneshwar R4
46	ICIRIAC 065	Survey on Natural Fibre Composite: Manufacturing Techniques, Mechanical Behaviour and Various Chemical Treatments	T Ramakrishnan, K Aravinth, Abhishek Singh, Deepak Raja S, Gokul Prasad C, Balasubramani
47	ICIRIAC 066	CHARACTERISATION OF MULTILAYER COATED CUTTING TOOLS IN TURNING OF STEELS – A REVIEW	Ganeshkumar S, Gokilakrishnan G, Dharanidharan.M, Manoj S, Gautam K
48	ICIRIAC 067	SMART TEACHABLE MULTI AGENT SYSTEM	Priya A and Dr. Vasudevan V
49	ICIRIAC 069	Plant Incubation System	S.Panneerselvam, Abhijith P R, Kavin Kumar R, Kavin Kumar R
50	ICIRIAC 070	Innovative Study on Friction Stir Welding	S.Panneerselvam and Kishore Ravichandran
51	ICIRIAC 072	MATHEMATICAL MODELING OF THIN LAYER DRYING CHARACTERISTICS OF OKRA (ABELMOSCHUS ESCULENTUS)	S. D. Sekar, S. Sekar, P. Duraimurugan, N. Mohanrajhu, S. Bharani Kumar, S. Rajesh
52	ICIRIAC 073	COMPREHENSIVE REVIEW OF TRANSFER LEARNING	Naveen Prabhu, Nithish Bharathi, Naveen R
53	ICIRIAC 074	Automatic Seed Disseminator	Nithya Priya S, Adhira M, Sowmiya Devi S, Sreeranjani S
54	ICIRIAC 076	Design and Fabrication of 5 Degrees of Freedom Robotic Arm	J.Indirapriyadharshini, Achitha M, Jahath Pranav R, Hemand Adish R
55	ICIRIAC 077	AI-POWERED CONTENT MODERATION	K. Vidhya, VS. Abhishek, G. Akash, S. Aravind Karti, R. Harshini,
56	ICIRIAC 079	Studies on developing a Humanoid Facial Expressive Robot	R. Manikandan, Victor R, Vishal S, Vishnu Prakash N
57	ICIRIAC 080	Single And Multi-Level DC-DC Converter For Electric Vehicles	Karre Mahesh, V Joshi Manohar, M. Dilip Kumar
58	ICIRIAC 081	Security Framework for Net Gun-Equipped Unmanned Aerial Vehicles	Kesavaraj K, Mithran N, Venkatesan M, Vinoth R , Dhamodharan N A and Swetha A

59	ICIRIAC 086	Ensemble Voting Machine Learning Model for Prediction of Campus Placement of the student	B.Kalaiselvi and Dr.S.Geetha
60	ICIRIAC 087	STUDIES ON PARTICLE SEPARATION EQUIPMENT- A REVIEW	S Venkatesh, M Kathirvel, R Vikram dharsan, K Yogaraju
61	ICIRIAC 090	Automatic Identification and classification of brain tumor using MRI images through transfer learning	K. Priyadharshini, Dr. M. Dhamodaran, S.Kaviyapriya, R.Harini, V.Kaviya, Dr. B. Ramasubramanian
62	ICIRIAC 091	DESIGN AND FABRICATION OF AIR PURIFIER & HUMIDIFIER USING WATER AS A FILTER	P.M.Arunkumar, S.Kannaki, A.Vimal Kumar, K.Selva Vignesh Hari haran, S.Vigneshwar, Ragu Nandhan S, Srisudharsanam
63	ICIRIAC 092	FOOD NUTRITION ANALYZER USING AI	Saranya N, Akhila B, Harini T, Hemalatha M A, Kaneshka Sre R S
64	ICIRIAC 093	MARINE OIL SPILL CLEANING ROBOT	K. Sheela Sobana Rani, Vignesh .G, Vignesh .S, Sanath Abhinav .S, Sumathi .S, Sindhuprabha .K
65	ICIRIAC 094	COMPONENT CARRYING AUTOMATED GUIDED VEHICLE	PRIYADHARSHINI R
66	ICIRIAC 095	Machinability Studies on Aluminium and its Alloys - A Literature Review	R. Suresh Kumar, K Alagu Vignesh, S. Gokulprasanth, A. Thillai Ambalanathan
67	ICIRIAC 096	Effect of velocity profile on pulsatile flow in macro blood vessels of a cardiovascular system	Karthick Sundaresan, KT.Gowtham, C.Ramcharan, J.Sudharshan ram, and K.H.Vaishnav
68	ICIRIAC 099	Influence of Fibers in Hybrid Polymer Composites fabricated by Hand lay-up Method	M. Mudhu Krishnan, R. Suresh Kumar, N. Jayanthi
69	ICIRIAC 109	SOCIAL NETWORK USERS MENTAL STRESS IDENTIFICATION USING MACHINE LEARNING	Aruna Subramanian and Shanthi Palaniappan, Navaneethakumar V M, Ravishankar S, Gopinath Selvamani
70	ICIRIAC 114	REMOVAL OF COLOUR FROM DYEING INDUSTRIES WASTE WATER USING ORGANIC & INORGANIC ABSORBENTS	A.Albert raj, Ragavarthni V,Rahini.P, Sahanaj Aneez M
71	ICIRIAC 117	Design And Fabrication Of Autonomous Robot Butler	D.Pritima, Neelash Kannan A, Krishnaprasath M, and udhaya raj J

72	ICIRIAC 119	Rural Built-Up Area Extraction from satellite Images Using Deep Neural Network	Shima Ramesh Maniyath and Leena K
73	ICIRIAC 120	Design and Development of a Submersible Robot	Kamalakannan, Vishnudhasan, Yuvanraj, Viveagh
74	ICIRIAC 121	Next-Generation Digital Healthcare Cloud Folder For Patients	Gayathri S, Thilagaraj M, Kothai.R, Indirapriyadharshini J, T.Sivaranjani
75	ICIRIAC 122	Six-Wheeled Material Handling Robot with 3-DOF Robotic Arm	R. Priyadharshini, D Nalini, Adithyaa Ramesh, Akshey PB and Ijas Ahamed A)

Department of Mechatronics Engineering
Sri Krishna College of Engineering and Technology
Kuniamuthur, Coimbatore - 641 008.

Dr. M. Lydia, M.E., Ph.D.,
Professor and Head
Department of Mechatronics Engineering
Sri Krishna College of Engineering and Technology
Kuniamuthur, Coimbatore - 641 008.

SRI KRISHNA COLLEGE OF ENGINEERING AND TECHNOLOGY

Kuniamuthur, Coimbatore. Tamil Nadu 641008

(An Autonomous Institution Affiliated to Anna University, Chennai)

MECHATRONICS ENGINEERING ASSOCIATION

14.2.2023	**International Seminar on "Intelligent Vehicular Networks and Communication"**	**Dr. Anand Paul Director, Connected Computing and Media Processing Lab, Kyungpook National University, South Korea.**

Invitation

SRI KRISHNA COLLEGE OF ENGINEERING AND TECHNOLOGY

Kuniamuthur, Coimbatore. Tamil Nadu 641008

(An Autonomous Institution Affiliated to Anna University, Chennai)

Photographs

Department of Mechatronics Engineering organized an International Seminar on **"Intelligent Vehicular Networks and Communication"** on 14.02.2023**.**

Resource person:

Dr. Anand Paul

Director,

Connected Computing and Media Processing Lab,

Kyungpook National University, South Korea.

Session Highlights:

- Dimensionality Reduction Techniques
- Couple Non negative Matrix Factorization
- Intelligent Transportation Systems
- Vehicular Network Model.

S.No	Name	Designation	Organization Name
1	K. MANIKANDAN	Student	Mechanical
2	Lavanya A	Assistant Professor	Rathinam technical campus
3	TEKI L V S SAI MEGHANA	Student	SHRI VISHNU ENGINEERING COLLEGE FOR WOMEN
4	Kannaki S	Associate Professor	Sri Krishna College Of Engineering And Technology
5	VEDHA VINODHA D	Assistant Professor	JCT College of Engineering and Technology
6	Dr.K.P.Yuvaraj	Assistant Professor	Sri Krishna College of Engineering and Technology
7	Ramesh Babu R	Assistant Professor	Karpagam Institute of Technology
8	J. Dhiyaneswaran	Assistant Professor	Sri Krishna College of Engineering and Technology
9	Dr.S.Balasubramani	Associate Professor	Sri Krishna College of Engineering and Technology
10	MADHANKUMAR S	Assistant Professor	Sri Krishna College of Engineering and Technology
11	S.VAJITHA NAZREEN	Assistant Professor	SKCET
12	Deepak kumar	Student	Sri Krishna College of engineering and technology
13	Dr. N. Mithran	Associate Professor	Sri Krishna College of Engineering and Technology
14	MOHANAPRIYA s	Assistant Professor	JCT College of Engineering and Technology
15	THAHSEEN THAHIR	Assistant Professor	JCT college of engineering and technology
16	RAGUL KANNAN R	Assistant Professor	Dhanalakshmi Srinivasan Engineering College (Autonomous)
17	ARUNKUMAR P M	Assistant Professor	Kongu Engineering College
18	Dr. R. Manikandan	Associate Professor	Sri Krishna College of Engineering and Technology
19	Dr.D.Pritima	Professor	Sri Krishna College of Engineering and Technology
20	Sindhu	Assistant Professor	Sri Krishna College of Engineering and Technology
21	Dr.K.Ganapriya	Assistant Professor	SSMIET
22	Dr.Saveetha.P	Professor	Nandha College of Technology

23	Dr.M.Bhuvaneswari	Assistant Professor	Sri Krishna College of Engineering and Technology
24	Akash Kumar	Student	International vehicular network and communication
25	J. LIDWINA JENNIFER	Assistant Professor	COIMBATORE INSTITUTE OF ENGINEERING AND TECHNOLOGY
26	ANANTHI K	Assistant Professor	Sri Krishna College of Engineering and Technology
27	A SURESH KUMAR	Assistant Professor	Rathinam Technical Campus
28	Suganyadevi D	Assistant Professor	Dr.Mahalingam college of engineering and technology pollachi
29	S Gospeline Christiana	Assistant Professor	Sethu Institute of Technology
30	GOWTHAMI D	Assistant Professor	NANDHA COLLEGE OF TECHNOLOGY
31	K. MANIKANDAN	Student	K. MANIKANDAN
32	Sivamani. S	Assistant Professor	E. G. S. P. E. C
33	G SATHYA	Assistant Professor	Tamilnadu college of Engineering
34	KARTHIKA S	Assistant Professor	BANNARI AMMAN INSTITUTE OF TECHNOLOGY
35	SANTHOSHKUMAR S P	Assistant Professor	Rathinam Technical Campus
36	Rajkumar T	Assistant Professor	Nandha College of Technology
37	Sakthivel G	Student	Mahendra institute of technology
38	SABARI.S	Student	Mahendra institute of technology
39	S.Sanjai krishnan	Student	Sanjai krishnan.s
40	Praveen Kumar.s	Student	Mahendra institute of technology
41	Nithesh Anand M S	Student	Sri Krishna college of engineering and technology
42	Dr.J.Indirapriyadharshini	Assistant Professor	SRI KRISHNA COLLEGE OF ENGINEERING AND TECHNOLOGY,COIMBATORE
43	BHARATHI B	Assistant Professor	Coimbatore Institute of Engineering and Technology
44	yoga R	Assistant Professor	Coimbatore institute of technology and engineering
45	Kanchana S	Assistant Professor	Coimbatore institute of engineering and technology
46	BHARATHI T K	Assistant Professor	Coimbatore Institute of Engineering and Technology

47	Pushpalatha	Assistant Professor	Coimbatore Institute of engineering and technology
48	Ganesh K	Student	Skcet
49	G.VEERAPPAN	Associate Professor	SRI KRISHNA COLLEGE OF ENGINEERING AND TECHNOLOGY
50	ENIYAVAN P	Student	Tamil Nadu Agricultural University
51	TAMILSELVAM	Student	Mahendra institute of technology
52	M Prabu	Assistant Professor	Nandha Engineering College
53	BHARANIDHARAN.J	Student	Sri Krishna College of engineering and technology
54	Ragavi Priya S	Assistant Professor	Sns College of Technology
55	KUMARASAN T	Assistant Professor	JJ COLLEGE OF ENGINEERING AND TECHNOLOGY
56	Adith U	Student	Sri Krishna Collage Of Engineering And Technology
57	GOKUL NILAVAN	Student	Sri Krishna College of engineering and technology
58	Hari Krishnan C	Student	SRI KRISHNA COLLEGE OF ENGINEERING AND TECHNOLOGY
59	BENJAMIN A	Student	Sri Krishna college of engineering and Technology
60	Abdul wahid J	Student	Skcet
61	BARANISUNDAR S	Student	SRI KRISHNA COLLEGE OF ENGINEERING AND TECHNOLOGY
62	S.JAYASURYA	Student	Sri krishna college of engineering and technology
63	VINOTH M	Assistant Professor	J J COLLEGE OF ENGINEERING AND TECHNOLOGY, TIRUCHIRAPPALLI
64	PAUL ANDERSON.G	Student	Jj college of engineering and technology
65	S SETTU	Assistant Professor	JCT COLLEGE OF ENGINEERING AND TECHNOLOGY
66	Dr.R.Prasanna lakshmi	Associate Professor	FATIMA MICHAEL COLLEGE OF ENGG & TECHNOLOGY
67	Dr.P.Padmanabhan	Professor	VV College of Engineering
68	SureshKumar.P	Assistant Professor	JCT college of Engineering and Technology Coimbatore

69	SIVASANKAR P	Student	THIAGARAJAR COLLEGE OF ENGINEERING
70	ABINITH R	Student	Sri krishna collage of engineering and technology
71	VIJAYA KUMAR R	Assistant Professor	Dr.N.G.P INSTITUTE OF TECHNOLOGY
72	RAGUL KANNAN R	Assistant Professor	Dhanalakshmi Srinivasan Engineering College (Autonomous)
73	Dr.S.Thirumalvalavan	Associate Professor	Arunai Engineering College
74	T. BOOPATHY	Assistant Professor	Dhanalakshmi Srinivasan Engineering College (Autonomous)
75	Santhosh S	Assistant Professor	JJ COLLEGE OF ENGINEERING AND TECHNOLOGY
76	Lakshminarayanan.S	Student	JJ college of engineering and technology
77	B.AVINASH	Assistant Professor	Coimbatore Institute of Engineering and Technology
78	Parthiban R	Assistant Professor	Coimbatore institute of engineering and technology
79	Deekshitha	Student	JJ college of engineering and technology
80	Sasi Rekha R	Student	Dhanalaksmi Srinivasan Engineering college
81	BHUVANESHWARI	Student	Dhanalakshmi Srinivasan Engineering college
82	ASHAYA K	Student	Dhanalakshmi srinivasan engineering college
83	Lidwina Jennifer J	Assistant Professor	CIET
84	NITHYA PRIYA S	Assistant Professor	Sri Krishna College of Engineering and Technology
85	Dr.V.Narasimharaj	Associate Professor	Sri Krishna College of Engineering and technology
86	G.VEERAPPAN	Associate Professor	Sri Krishnan College of Engineering and Technology
87	M Lydia	Professor	Sri Krishna College of Engineering and Technology
88	Dr. G. Edwin Prem Kumar	Professor	Sri Krishna College of Engineering and Technology
89	Bhuvaneswari M	Assistant Professor	Sri Krishna College of engineering and technology
90	R Priyadharshini	Assistant Professor	Sri Krishna College of Engineering and Technology, Coimbatore
91	Dr S.BALASUBRAMANI	Associate Professor	Sri Krishna College of Engineering and Technology

92	Dr. SELVAN T A	Professor	Sri Krishna College of Engineering and Technology
93	Dr. L Feroz Ali	Associate Professor	Sri Krishna College of Engineering and Technology
94	Dr M Vigneshkumar	Assistant Professor	Sri krishna college of Engineering and Technology
95	Ebinesan	Student	JJ COLLEGE OF ENGINEERING AND TECHNOLOGY
96	Ulaganathan.u	Student	JJ college of engineering and technology
97	SURAJ R A	Student	J J COLLEGE OF ENGINEERING AND TECHNOLOGY
98	Manikandan S	Student	J.J College of Engineering and Technology
99	Radhika. N	Student	N
100	R.pandi selvi	Student	International seminar on intelligent vehicular network and communication
101	Shanmuga Gukan	Student	JJCET
102	Logapranav C B	Student	Sri krishna college of engineering and technology
103	Bharanidharan N	Student	Sri krishna college of engineering and technology
104	HARI KRISHNAN C	Student	SKCET
105	Logapriyan M	others	Skcet
106	SANTHOSHKUMAR S P	Assistant Professor	Rathinam Technical Campus
107	M.Sureshkumar	Assistant Professor	St.Joseph's College of Engineering and Technology
108	yogeshvaran k	Assistant Professor	COIMBATORE INSTITUTE OF ENGINEERING AND TECHNOLOGY
109	Dr.K.P.YUVARAJ	Assistant Professor	SRI KRISHNA COLLEGE OF ENGINEERING AND TECHNOLOGY
110	Dhiyaneswaran J	Assistant Professor	Sri Krishna College Of Engineering and Technology
111	A. Deepak varma	Student	J.J College of engineering and technology

SRI KRISHNA COLLEGE OF ENGINEERING AND TECHNOLOGY

Kuniamuthur, Coimbatore. Tamil Nadu 641008

(An Autonomous Institution Affiliated to Anna University, Chennai)

Sample certificate:

SRI KRISHNA

COLLEGE OF ENGINEERING AND TECHNOLOGY

(An Autonomous Institution, Affiliated to Anna University, Chennai)
Kuniamuthur, Coimbatore – 641 008

DEPARTMENT OF MECHATRONICS ENGINEERING
in association with
KYUNGPOOK NATIONAL UNIVERSITY, South Korea

CERTIFICATE OF PARTICIPATION

This is to certify that Dr./Mr./Mrs. V. M. Bhuvaneshwari
of M. E communication systems has participated in International Seminar on **"Intelligent Vehicular Networks And Communication"** conducted by Department of Mechatronics Engineering on 14 Feb 2023 at Sri Krishna College of Engineering and Technology, Coimbatore.

Dr.M.Lydia
HoD/MCT

Dr.J.Janet
Principal

Department of Mechatronics Engineering
Sri Krishna College of Engineering and Technology
Kuniamuthur, Coimbatore - 641 008.

Dr. M. Lydia, M.E., Ph.D.,
Professor and Head
Department of Mechatronics Engineering
Sri Krishna College of Engineering and Technology
Kuniamuthur, Coimbatore - 641 008.

Materials Research. 2022; 25:e20210390
DOI: https://doi.org/10.1590/1980-5373-MR-2021-0390

Surface Modification of Strenx 900 Steel Using Electrical Discharge Alloying Process with Cu-10Ni- Cr_xPowder Metallurgy Sintered Electrode

S. Sridhar[a] , ***Srinivas Viswanth Valeti[b]***, ***Vishwanath Koti[c]***, ***S. Sathish[d]***, ***R. Raghu Chand[e]***,

N.S. Sivakumar[f], ***Mahesh. M[g]***, ***Ram Subbiah[h]*** , ***G. Veerappan[i]***

[a]*PSNA College of Engineering and Technology,Department of Mechanical Engineering, Dindigul.*
[b]*Aditya Engineering College, Department of Mechanical Engineering, Andhrapradesh.*
[c]*Ramaiah Institute of Technology, Department of Mechanical Engineering, Bangalore.*
[d]*Ramakrishna Engineering College, Department of Mechanical Engineering, Coimbatore*
[e]*Karavali Institute of Technology, Department of Mechanical Engineering, Mangalore.*
[f]*TISHK International University, Department of Mechatronics Engineering, Iraq.*
[g]*Guntur Engineering College, Department of Mechanical Engineering, Andhra Pradesh.*
[h]*Gokaraju Rangaraju Institute of Engineering and Technology, Department of Mechanical Engineering, Hyderabad.*
[i]*Sri Krishna College of Engineering and Technology, Department of Mechatronics Engineering, Coimbatore.*

Received: July 29, 2021; Revised: December 04, 2021; Accepted: December 28, 2021

The present investigation aims to coat the layer with Nickel (Ni) and Copper (Cu)over the surface of strenx 900 steel using semi sintered Cu-10Ni-Cr_x electrodes(x = 2, 4 & 6 wt. %). Three different proportions of semi sintered electrodes such as, Cu-10Ni-2 weight percentage of Chromium (Cr), Cu-10Ni-4 wt. % Cr,and Cu-10Ni-6 wt. % Cr were prepared by powder metallurgy route. Electric discharge alloying was completed based on L_9 orthogonal array and alloyed parameters were optimized using Taguchi method. The alloyed surfaces were characterized using scanning electron microscope and atomic force microscopy. The deposition of formation of intermetallic was studied using X- ray diffractometer. Higher Material Transfer Rate (MTR) was obtained at 9A, 350A and 6% chromium using Cu-10 Ni-Cu electrode. The chromium percentage was the foremost factor on Surface Roughness (SR) (73.71%) and MTR(96.56%). From Taguchi approach, the minimum SR was attained at percentage of chromium of 2%, compaction pressure of 250 Megapascal (MPa) and peak current of 9A. The maximum MTR was achieved at 6 percentage of Cr, compaction pressure of 350 MPa and peak current of 3A. Wear loss for Cu-10 Ni-Cr increases linearly with increase in sliding speed from 2m/s to 4m/s respectively.

Keyword: *Electrical discharge alloying, Powder Metallurgy, Taguchi, Characterization, Atomic force microscopy.*

1. Introduction

Electrical discharge machining is an unconventional machining process that involves eroding material from a work piece using a tool called electrode. The process occurs as a sequence of electrical discharges in the presence of dielectric fluid[1]. In case of die sinking Electric Discharge Machining (EDM), the process should be carried out only with the dielectric fluids such as de ionized water; kerosene and EDM oil[2]. EDM process is a suitable technique inmanufacturingof micro holes. It is also an economic, quick and cost effective for producing holes in hard and soft materials[3]. The undesirable layer was formed after machining known as recast layer which is inevitable but could be controlled by varying EDM process parameters. The harder recast layers, on the other hand are helpful in improving the wear resistance, as demonstrated by deliberate surface alloying during EDM. The use of partially sintered Powder Metallurgy (PM) electrodes, EDM in a metal powder suspended dielectric are the most popular methods for performing alloying during EDM that were been widely adopted in the past[4]. The common methods of surface modification using EDM is carried out by two means such as, use of semi sintered electrode and mixing powder in dielectric[5]. The surface texture effects were based on the level of control factors[6]. By using Powder metallurgy tool electrodes, EDM tooling costs can be reduced while tool electrodes can be produced in more quantity[7]

The surface of mould and tools has to be modified in order to increase their service life as well as withstand corrosion. Nevertheless, high machine price and complex processes makes to analyze novel surface modification processes[8]. During EDM of powder metallurgy of Cu-Zn, it was found that more contamination of dielectric medium was obtaineddue to the release of more copper powder from electrode. Poor surface

*e-mail: sri_2855@yahoo.co.in

topology was obtained due to the frequent occurrences of short circuits and arcs. It was pointed out that machining stability got affected more with increase in copper powder size[9].Powder metallurgy of Cu-Cr electrode yielded low Material Removal Rate (MRR), higher electrode wear ratio and high surface roughness, but electrolytic Cu electrode was better in achieving high MRR than powder metallurgy of Cu-Cr[10]. EDM of Titanium Aluminium Vanadium (Ti–6Al–4V) alloy with powder metallurgy of Cu–Tantalum Carbide (TaC) electrode in urea solution dielectric yielded in the deposition of nitrides, carbides, oxides of titanium and tantalum on the substrate. The base surface hardness improved from 316 Vicker Hardness (HV) to 902 HV[11].During machining carbon steel by suspending tungsten and titanium powders in kerosene dielectric, formation of Titanium Carbide (TiC) and Tungsten Carbide (WC) were identified on substrate due to the reaction between decomposed carbon with titanium and tungsten powders[12].

Very few researchers have carried out investigation on Electric Discharge Alloying (EDA) using Cu-Ni-Cr on strenx 900 steel. This investigation focuses on synthesis ofpowder metallurgy of Cu-10Ni-Cr_x electrodes produced at three different mixing ratios (2, 4, and 6 wt. % Cr), compaction pressure (250, 300, and 350MPa) and peak current (3A, 6A and 9A).

2. Materials and Methods

2.1. Preparation of PM semi sintered Cu-10Ni-Cr$_x$ electrode

The elemental powders of copper, nickel and chromium were mixed in addition of polyvinyl alcohol using ball mill for 1 hour. The ratio of ball to powder is 10:1. The hydraulic press of 150kN was used to compact of copper, nickel, and chromium. Three different compaction pressureswere applied with 250, 300 and 350MPa for preparing the electrode. Constant hydraulic forces were applied for 10min using punch and then pallet was ejected using lab press. The compacted cylindrical billet dimension with 10mm diameter and 20mm length were obtained. The tubular furnace was brought to vacuum and the compacted specimens were heated in tubular furnace containing argon atmosphere and the heating rate for sintering is 10°C per min. The furnace temperature for sintering wasdone at 800°C and further, it was cooled down inside the furnace to achieve homogenous mixture of powder materials.

2.2. Surface modification of strenx steel

The sintered alloys were coated on thesurface of strenx steel plate. The substance compositions of the strenx steel were shown in Table 1.The positive polarity was applied to sintered electrode.The process parameters were shown in Table 2. By varying parameters, alloycharacteristics were analyzed. An L_9 orthogonal array was used for conducting the experiment which is shown in Table 3. Surface roughness was measured using Mitutoyo SJ-400 tester over the alloyed surface. The surface topology of the modified layer was investigated using SEM with Energy Dispersive X-Ray Spectroscopy (EDS). Further, the alloyed surface was analyzed using atomic force microscopy.

2.3. Wear measurement

The pin substrates were alloyed by using three electrodes namely Cu-10Ni-2 wt. %, Cu-10Ni-4 wt. %, and Cu-10Ni-6 wt %. Wear test was conducted using tribometer of American Society for Testing and Materials (ASTM): G99-05. The pin was made to rotate against EN31 steel disc of 100mm diameter. The weight loss of the pin was measured using 0.1 mg precision electronic weighing balance.

Table 1. Substance composition of Strenx steel.

C	Si	Mn	P	S	Cr	Cu	Ni	Mo	B	Fe
0.20	0.50	1.60	0.020	0.010	0.80	0.3	2	0.70	0.005	remaining

Table 2. Control factors and their levels.

Machining Condition	Description
Work piece	Strenx 900 Steel
Electrode material	Cu-Ni-Cr
Dielectric	EDM oil 30
Polarity	Strenx 900 rectangular plate: Negative Copper tool: Positive
Process parameter with their levels	
Peak current	3A, 6A, 9A
Compaction pressure	250 Mpa, 300Mpa, 350Mpa
semi sintered electrode	Cu-10Ni-Cr_x
Constant Parameters	
Gap Voltage (V)	50
Duty factor	50%
Spark Gap	0.10mm
Flushing pressure	0.8 kg/cm^2

3. Results and Discussion

3.1.Surface morphology of alloyed surface

Figure 1a-b shows the surface morphology of alloyed surface. The lesser amount of nickel and chromium were deposited over the surface of strenx steel. The electrode material suspended in EDM 30 oil moved to the surface while applying peak current. Better surface roughness was obtained due to the positive polarity of the electrode and current density on anode is smaller than that on the cathode due to the superior radius of discharge mark on the anode[13]. From Figure 1b, it was evident that higher current discharge (9A) has produced craters along with deposition of nickel

Table 3. Experimental observations.

S.No	Wt. % of Cr	Compaction pressure MPa	Peak current A	SR µm	MTR mg/min
1	2	250	3	5.9177	91.60
2	2	300	6	6.5000	107.00
3	2	350	9	6.7611	110.40
4	4	250	6	6.6777	190.00
5	4	300	9	7.1000	208.50
6	4	350	3	7.6111	230.80
7	6	250	9	7.4377	281.23
8	6	300	3	7.9494	311.20
9	6	350	6	8.3711	329.70

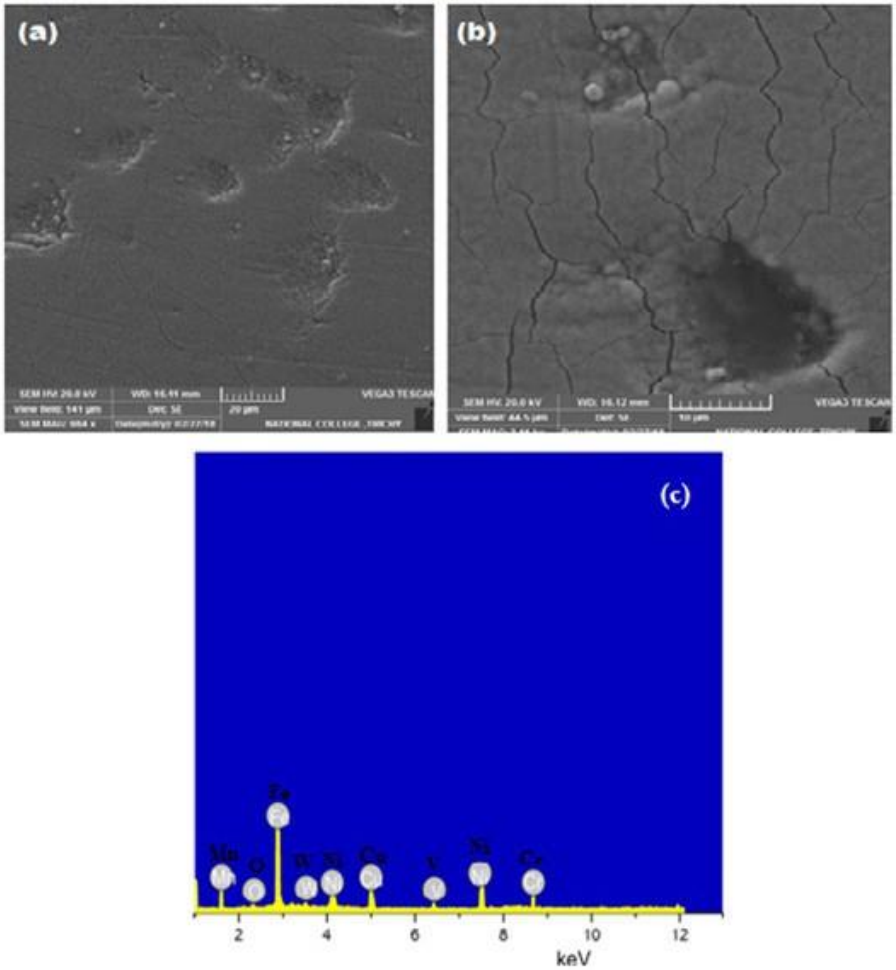

Figure 1. Scanning Electron Microscope (SEM) analysis of alloyed surface by Cu-10Ni-2Cr at (a) peak current of 6A, compaction pressure of 300 MPa and 2 wt.% Cr (b) peak current of 9A, compaction pressure of 250Mpa and 6 wt.% Cr(c) EDS result of modified layer using Cu-10Ni-2Cr.

and chromium. The formation of surface crack was obtained due to immediate quenching of fused metal in localization area. Figure 1c shows EDS result of the alloyed layer using Cu-10Ni-2Cr. The nickel depositions were confirmed with corresponding peaks of nickel adjacent to ferrous peak.

Figure 2 shows the SEM and EDS results of alloyed layer. The evidence of materials deposited from tool electrode wasshown in EDS results. It was evident that surface of strenx steel was coated with nickel and chromium. EDS results has confirmed the deposition of chromium and nickel over surface. Higher percentage of Cr has improved the alloy content andusing semi sinteredCu-10Ni-6Cr electrode, Cu powder improves binding strength as well as conductivity for EDM machining. The addition of alloying element has both lower electrical conductivity as well as thermal conductivity in powder metallurgy electrode. The rates of erosion wasincreased and as a result, tool material got deposited on the substrate[14].

3.2. Surface morphology of atomic force microscopy

Figure 3a shows the surface topology obtained at peak current of 3A and compaction pressure of 250MPa. Atomic force microscopy results revealed better surface finish which

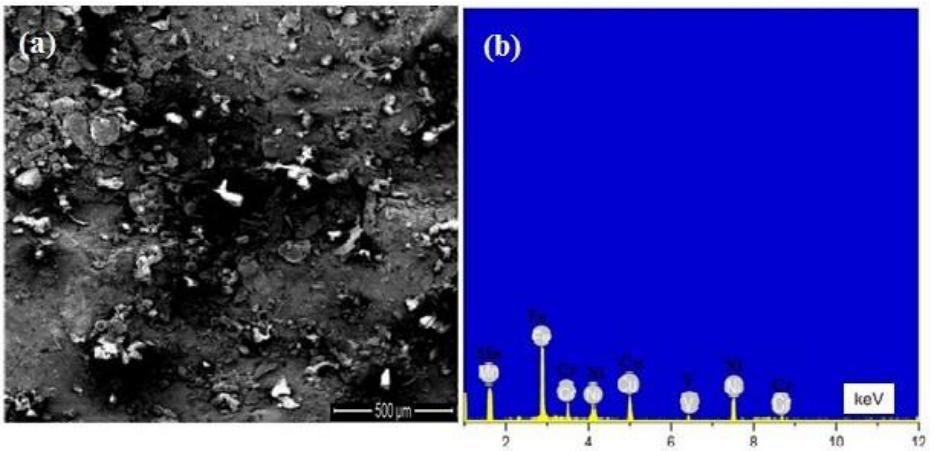

Figure 2. (a) SEM and (b) EDS result of the alloyed layer using Cu-10Ni- 6Cr at peak current of 9A, compaction pressure of 250Mpa and 6 wt.% Cr.

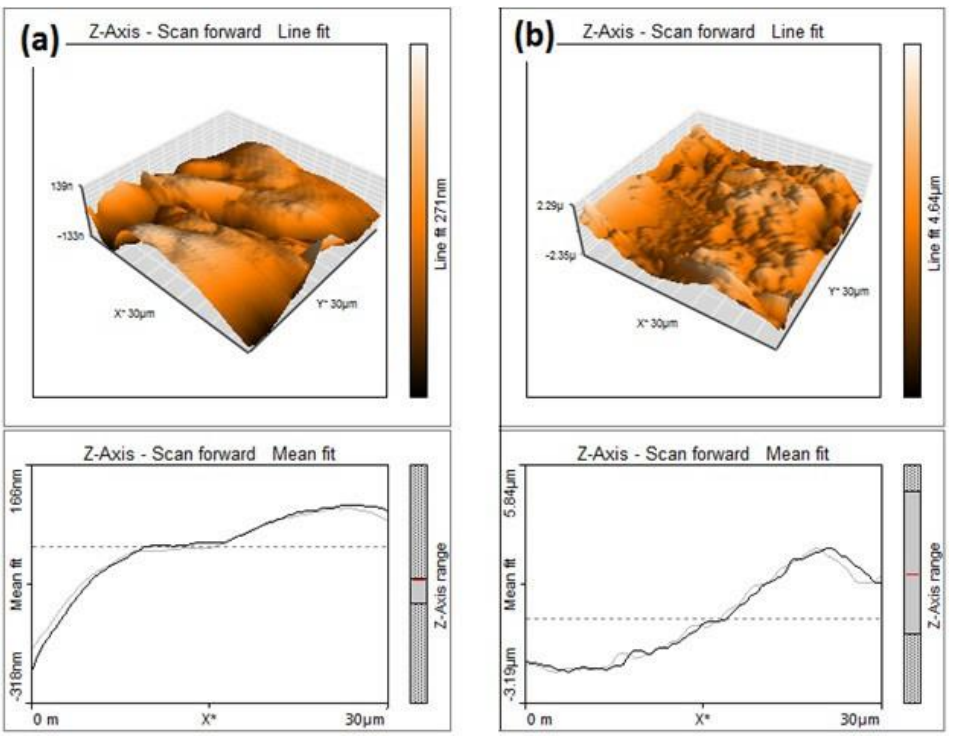

Figure 3. Atomic force microscopy results for the coated layer obtained (a) 3A, compaction pressure of 250 MPa and Cu-10Ni-2% Cr electrode (b) 6A, compaction pressure of 350 MPa and Cu-10Ni-6% Cr electrode.

has no peaks and troughs. This finish was obtained due to the two reasons (a) the low compaction pressure which results in loose bonding of electrode particles and (b) nickel prevents secondary arcing which results in uniform discharge causes lower surface roughness[15].

Figure 3b shows the surface topology obtained at peak current of 6A and compaction pressure of 350MPa. At this set of parameters, high surface roughness was obtained due to deposition of more alloying elements of nickel and chromium.The reverse polarity of electrode causes to form more discharge energy which results in more alloying particles of electrode to fall on the work piece. These alloyed particles become bonded to the work piece during cooling by flush system[16]. High chromium content released from electrode material forms bridging effect.

3.3. ANOVA results

From Table 4 and 5, Analysis of variance (ANOVA) results revealed that chromium content in electrode is the foremost in affecting surface roughness as well as material transfer rate, followed by compaction pressure. Therefore, chromium content and compaction pressure are the significant parameters towards SR and MTR. The higher chromium content improved MRR has reduced the electrode wear and enhanced the surface roughness[17]. The influential percentage contribution of chromium content, compaction pressure and peak current towards SR was found to be73.71% and 25.93% and it's shown in Table 4. Table 5 shows ANOVA results of material transfer rate. The influential percentage contribution of chromium content, compaction pressure and peak current towards SR were found to be 96.56% and 3.03% respectively. R- Squared values were closer to unit which makes model significant. Higher Material transfer rate was obtained at 9A, 350 MPa using 6% of chromium.

3.4. Wear measurement

Figure 4 shows the wear characteristics of prepared Cu-10 Ni-Cr_x electrode. PM Cu-10 Ni without chromium content shows high wear compared to Cu-10 Ni-Cr_x (x=2, 4 and 6 wt. % Cr). The wear loss increase steadily with an increase in sliding speed from 2m/s to 6m/s. Wear loss for PM Cu-10 Ni-Cr_0 is high compared to the other alloy added with chromium. Wear loss for Cu-10 Ni-Crincreases linearly with an increase in sliding speed from 2m/s to 4m/s. With

Table 4. Variance analysis for SR.

Source /SR	DF	SS	MS	F	P	%
% of Cr	2	3.49656	1.74828	612.33	0.002	73.71
Compaction pressure	2	1.22997	0.61499	215.40	0.005	25.93
Peak current	2	0.01107	0.00554	1.94	0.340	00.23
Error	2	0.00571	0.00286	--	--	00.13
Total	8	4.74332	--	--	--	100
S= 0.0534336	R-sq= 99.88%		R-sq(Adj)= 99.52%		R-sq(Pred)= 97.56%	

Table 5. Variance analysis for MTR.

Source /MTR	DF	SS	MS	F	P	%
% of Cr	2	62696.7	31348.3	1123.06	0.001	96.56
Compaction pressure	2	1968.0	984.0	35.25	0.028	03.03
Peak current	2	208.2	104.1	3.73	0.211	00.32
Error	2	55.8	27.9	--	--	00.09
Total	8	64928.7	--	--	--	100
S= 5.28330	R-sq= 99.91%		R-sq(Adj)= 99.66%		R-sq(Pred)= 98.26%	

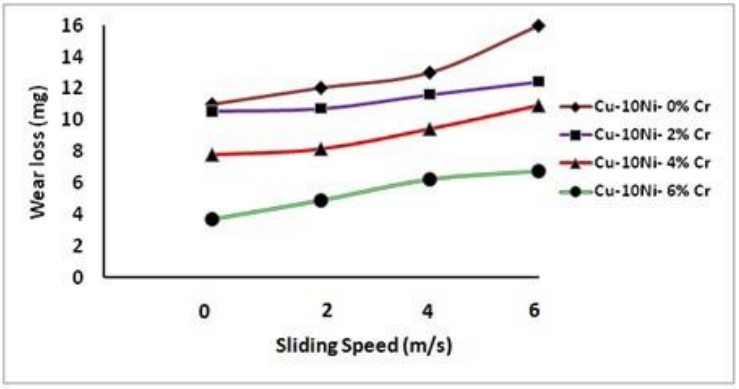

Figure 4. Wear behaviors of Cu-Ni-Cr.

subsequent increase in sliding speed from 4m/s to 6m/s, there were no substantial loss in wear due to increase in chromium content. Sliding speed was the predominant factor to affect the wear rate in powder metallurgy based copper nickel alloy[18]. The wear characteristics were found in magnesium alloy at different temperature conditions[19].

4. Surface Roughness

The desirable SR value is found out from Taguchi approach. Based on the experimental objective, the SR value should be minimized. The surface roughness and its properties were enhanced through material deposition to the base alloys[20,21]. As per condition of the outcome, the lower the better is considered for SR. According to the criteria, Signal to Noise (SN) ratio and means are computed and it's shown in Table 6. SN ratio was used to reduce the error in design of experiment and uncertainty factors[22]. The quality characteristics and its effect on the responses were depends on SN ratio[23]. The significant factor of the process and its predicted model were controlled by SN ratio[24].

Figure 5 shows that the main causes of SN ratio on SR. From the graph, the desirable SR value is attained at the level of $A_1B_1C_3$. Therefore, the minimum SR is attained at percentage of chromium of 2%, compaction pressure of 250MPa and peak current of 9A.

5. Material Transfer Rate

The aim of the investigation is to increase the material transfer rate. Hence, maximize the better criteria waschosen to achieve the MTR. Based on this condition, the mean and SN ratios are estimated and it's listed on the Table 7. The optimal MTR is shown in Figure 6. The desirable MTR is obtained at $A_3B_3C_1$. Therefore, the maximum MTR is achieved at percentage of Cr of 6, compaction pressure of 350 MPa and peak current of 3A.The effect of compaction pressure on material transfer rate were investigated for

Table 6. Calculated SN ratio and means for SR

	SN ratio			Means		
Level	% of Cr	Compaction pressure	Peak current	% of Cr	Compaction pressure	Peak current
1	-16.10	-16.45	-17.03	6.393	6.678	7.159
2	-17.05	-17.10	-17.07	7.130	7.183	7.183
3	-17.96	-17.56	-17.02	7.919	7.581	7.100
Delta	1.86	1.11	0.05	1.526	0.903	0.083
Rank	1	2	3	1	2	3

Table 7. Calculated SN ratio and means for MTR.

	SN ratio			Means		
Level	% of Cr	Compaction pressure	Peak current	% of Cr	Compaction pressure	Peak current
1	40.23	44.60	45.45	103.0	187.6	211.2
2	46.41	45.61	45.51	209.8	208.9	208.1
3	49.73	46.16	45.41	307.4	223.6	200.0
Delta	9.51	1.56	0.10	204.4	36.0	11.2
Rank	1	2	3	1	2	3

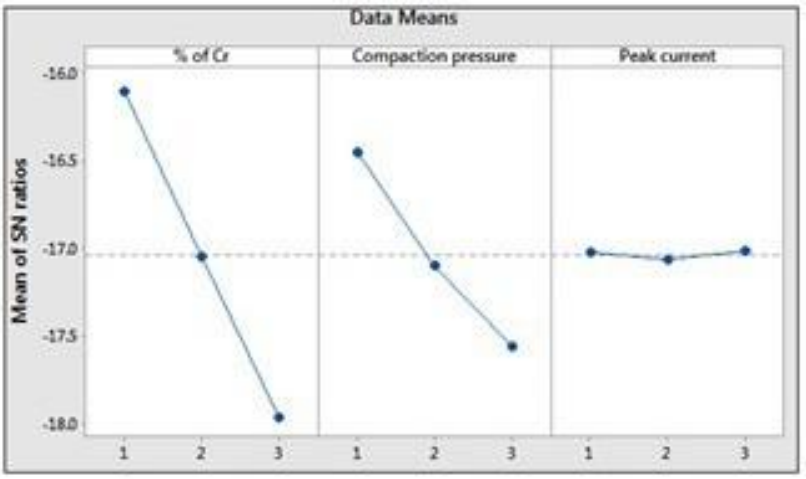

Figure 5. Desirable factor for SR.

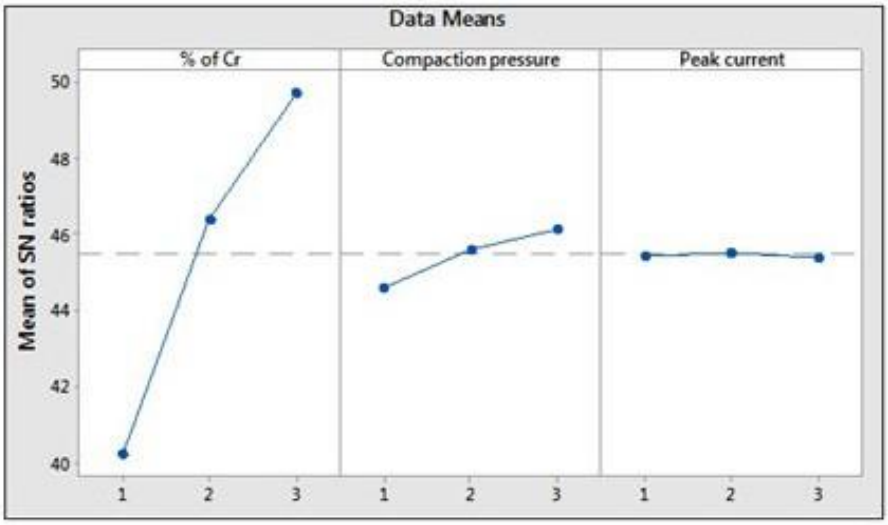

Figure 6. Desirable factor for MTR.

different alloys with forming temperature conditions[25]. The processing parameters and dynamic compaction system were played an essential role in material transfer rate[26].

6. Conclusion

- Chromium, copper and nickel were deposited successfully over Strenx 900 steel using EDA process.
- Higher material transfer rate was obtained at 9A, 350A and 6% chromium using Cu-10 Ni-Cu_6 electrode.
- EDS results revealed the presence of nickel, chromium and copper over Strenx steel 900.
- Strenx steel surface alloyed using Cu-10 Ni-Cu_6 electrode showed less wear compared to the other synthesized electrode. Additon of chromium content in PM electrode has enhanced the wear resistance.
- Higher material transfer rate yielded in higher surface roughnesswere witnessed by peaks and troughs in atomic force microscopy analysis.
- Chromium content is the foremost factor in influencing material transfer rate and surface roughness followed by compaction pressure.
- From variance analysis, percentage of chromium was identified with dominant factor for SR (73.71%) and MTR (96.56%).
- From Taguchi approach,the minimum SR was attained at percentage of chromium of 2%, compaction pressure of 250Mpa and peak current of 9A.
- The maximum MTR is achieved at percentage of Cr of 6, compaction pressure of 350 MPa and peak current of 3A.

7. References

1. Puertas I, Luis CJ. A study of optimization of machining parameters for electrical discharge machining of boron carbide. Mater Manuf Process. 2004;19(6):1041-70.
2. Liu Y, Chang H, Zhang W, Ma F, Sha Z, Zhang S. A simulation study of debris removal process in ultrasonic vibration assisted electrical discharge machining (EDM) of deep holes. Micromachines. 2018;9(8):378. https://doi.org/10.3390/mi9080378.
3. Marichamy S, Saravanan M, Ravichandran M, Veerappan G. Parametric optimization of electrical discharge machining process on alpha beta brass using grey relational analysis. J Mater Res. 2016;31(16):2531-7.
4. Arun I, Vaishnavi P, Duraiselvam M, Senthilkumar V, Anandakrishnan V. Development of carbide intermetallic layer by electric discharge alloying on AISI-D2 tool steel and its wear resistance. Int J Mater Res. 2014;105(6):544-51.
5. Muttamara A, Kanchanomai C. Effect of carbon in the dielectric fluid and workpieces on the characteristics of recast layers machined by electrical discharge machining. Metall Mater Trans, A Phys Metall Mater Sci. 2016;47(6):3248-55.
6. Guu YH, Hou MTK. Effect of machining parameters on surface textures in EDM of Fe-Mn-Al alloy. Mater Sci Eng: A. 2007;466(1-2):61-7.
7. Naveen B, Maheshwari S, Sharma C. Performance evaluation of powder metallurgy electrode in electrical discharge machining of AISI D2 steel using Taguchi method. Int J Aerospace Mech Eng. 2008;2(3):167-71.
8. Chen YF, Chow HM, Lin YC, Lin CT. Surfacemodification using semi-sintered electrodes on electrical discharge machining. Int J Adv Manuf Technol. 2008;36(5-6):490-500.
9. Samuel MP, Philip PK. Powder metallurgy tool electrodes for electrical discharge machining. Int J Mach Tools Manuf. 1997;37(11):1625-33.
10. Gulcan O, Uslan I, Usta Y, Çogun C. Effect of use of Cu–Cr P/M electrodes on machining performance of electric discharge machining. J Fac Eng Archit Gaz. 2015;30(3):381-94.
11. Ndaliman MB, Khan AA, Ali MY. Formation of nitrides and carbides on titaniumalloy surface through EDM. Adv Mat Res. 2012;576:7-10.
12. Furutani K, Saneto A, Takezawa H, Mohri N, Miyake H. Accretion of titanium carbide by electrical discharge machining with powder suspended in working fluid. Precision Eng. 2001;25(2):138-44.
13. Rao PS, Purnima NS, Prasad DS. Surface alloying of D2 steel using EDM with WC/Co P/M electrodes made of Nano and Micron sized particles. Mater Res Express. 2018;6(3):036511.
14. Arun I, Yuvaraj C, Madhu A, Ramesh T. A comparison on microstructure and mechanical properties of electric discharge

metal matrix nickel and silica composite coating on duplex stainless steel. J Compos Mater. 2021;55(4):002199832095388. https://doi.org/10.1177/0021998320953882.

15. Bai CY, Koo CH. Effects of kerosene or distilled water as dielectric on electrical discharge alloying of superalloy Haynes 230 with Al-Mo composite electrode. Surf Coat Technol. 2006;200(12-13):4127-315.
16. Gill AS, Kumar S. Surface characteristics investigations of tool steel machined by powder metallurgy tool in EDA. Mater Res Express. 2019;6:1-14.
17. Gulcan O, Uslan I, Usta Y, Çogun C. Effect of use of Cu–Cr P/M electrodes on machining performance of electric discharge machining. J Fac Eng Archit Gaz. 2015;30(3):381-94.
18. Cheng J, Gan X, Li Z, Lei Q, Zhou K. Wear map for sliding wear behavior of Cu-15Ni-8Sn alloy against bearing steel under oil-lubricated condition. J Cent South Univ. 2020;27(2):311-24. http://dx.doi.org/10.1007/s11771-020-4297-y.
19. An J, Zhang YX, Lv XX. Tribological characteristics of Mg-3Al-0.4Si-0.1Zn alloy at elevated temperatures of 50-200 °C. Tribol Lett. 2018;66:14.
20. Góral A, Lityńska-Dobrzyńska L, Kot M. Effect of surface roughness and structure features on tribological properties of electrodeposited nanocrystalline Ni and Ni/Al2O3 coatings. J Mater Eng Perform. 2017;26(5):2118-28.
21. Góral A. Nanoscale structural defects in electrodeposited Ni/Al2O3 composite coatings. Surf Coat Tech. 2017;319:23-32.
22. Moayyedian M, Derakhshandeh JF, Said S. Experimental investigations of significant parameters of strain measurement employing Taguchi method. SN Appl Sci. 2019;1(1):92.
23. Md-Ralib AA, Mortada O, Orlianges JC, Crunteanu A, Chatras M, Nordin AN. J Mater Sci Mater Electron. 2017;28(1):9132-8. http://dx.doi.org/10.1007/s10854-017-6647-6.
24. Baligidad SM, Chandrasekhar U, Elangovan K, Shankar S. Taguchi's Approach: design optimization of process parameters in selective inhibition sintering. Mater Today. 2018;5(2 Pt 1):4778-86. http://dx.doi.org/10.1016/j.matpr.2017.12.051.
25. Radchenko AK. Mechanical properties of green compacts. II. Effect of powder relative bulk density on the strength of compacts with different forming temperature conditions. Powder Metall Met Ceramics. 2004;43(11-12):552-63.
26. Sethi G, Myers NS, German RM. An overview of dynamic compaction in powder metallurgy. Int Mater Rev. 2008;53(4):219-34. http://dx.doi.org/10.1179/174328008X309690.

Journal of Alloys and Compounds 958 (2023) 170500

Contents lists available at ScienceDirect

Journal of Alloys and Compounds

journal homepage: www.elsevier.com/locate/jalcom

Effects of ZnO addition on the microstructure/corrosion, wear and mechanical properties of sintered Mg-Al matrix composites

S. Jayasathyakawin [a], M. Ravichandran [a,b,*], Sikiru Oluwarotimi Ismail [c,*], G. Veerappan [d]

[a] Department of Mechanical Engineering, K. Ramakrishnan College of Engineering, Samayapuram, Trichy 621112, Tamil Nadu, India
[b] Visiting Professor, Department of Mechanical Engineering & University Centre for Research & Development, Chandigarh University, Mohali-140413, Punjab, India
[c] Department of Engineering, Centre for Engineering Research, School of Physics, Engineering and Computer Science, University of Hertfordshire, Hatfield AL10 9AB, UK
[d] Department of Mechatronics Engineering, Sri Krishna College of Engineering and Technology, Coimbatore 641008, Tamil Nadu, India

ARTICLE INFO

Article history:
Received 1 March 2023
Received in revised form 1 May 2023
Accepted 8 May 2023
Available online 9 May 2023

Keywords:
Magnesium
Composite
Powder metallurgy
Mechanical properties
Corrosion
Wear, Friction

ABSTRACT

Magnesium (Mg)-based composites offer outstanding properties, which make them suitable materials for various applications in medical, aerospace and energy sectors, among others. The wide applications of Mg-based composites have attracted continuous effort to increase their properties and performances. Therefore, the present work focused on synthesizing magnesium-aluminium-zinc oxide (Mg-Al-ZnO) composites. Mg-3Al-xZnO (x = 3, 6 and 9 wt%) composites were prepared using powder metallurgy (PM) route. The composite powders and sintered composites were analyzed to determine their microstructures, using scanning electron microscopy (SEM) and energy dispersive X-ray (EDX) analysis. In addition, the sintering process took place in argon atmosphere at 450 °C. The quantitative analyses of density, porosity, hardness, compressive strength (CS) and corrosion rate (CR) of the composites were performed. Wear performance was also studied with various wear control parameters, such as the sliding velocity (V), sliding distance (D), applied load (P) as well as ZnO content. Pin-on-disc apparatus was used to determine the wear rate (W*R*) and coefficient of friction (COF) of the innovatively prepared Mg-3 wt%Al-ZnO composites. The experimental study was conducted in accordance with Taguchi's L_{16} orthogonal design. Signal-to-noise (S/N) ratio analysis was employed to determine the best combination of parameters for W*R* and COF. Summarily, SEM images confirmed that ZnO particles were uniformly distributed in the composite samples. Statistical technique, called analysis of variance (ANOVA), was adopted to find the significant factor which affected W*R* and COF. The P significantly affected the W*R*, followed by the inclusion of ZnO. But, with respect to COF, ZnO reinforcement inclusion affected COF significantly when compared with the P. Both V and D did not affect W*R* and COF. Hence, the application of the various composite samples should depend on their various responses to friction and wear, especially in working conditions where both quantities are inevitable.

© 2023 Elsevier B.V. All rights reserved.

1. Introduction

Composite materials have better properties that depend on several factors, such as the matrix, reinforcement materials, interfaces between materials, volume fraction and temperature [1]. Metal matrix composites (MMCs) are commonly used in the wear resistant materials. Also, they have major applications in automotive components, such as piston rings, brake discs, brake rotors and cylindrical linings.

MMCs possess superior properties, including strength, stiffness and creep resistance. The automotive industry appreciates lighter materials to decrease weight and improve fuel efficiency [2]. Lightweight oxides and carbides are considered as best reinforcements for MMCs, due to their high strength, low density, high Young's modulus and low chemical reaction [3]. In contrast to other metallic materials, magnesium (Mg) and its alloys can be used in the spacecraft and vehicle industries to support more fuel economy [4]. For the applications that require load bearing and strength, these lightweight materials are reinforced with high strength materials [5].

* Corresponding author at: Department of Mechanical Engineering, K. Ramakrishnan College of Engineering, Samayapuram, Trichy 621112, Tamil Nadu, India.
E-mail addresses: smravichandran@hotmail.com (M. Ravichandran), s.ismail3@herts.ac.uk (S.O. Ismail).

https://doi.org/10.1016/j.jallcom.2023.170500
0925-8388/© 2023 Elsevier B.V. All rights reserved.

There have been several studies on the properties of Mg matrix composites, which demonstrated their higher strengths than single Mg alloys [6]. Numerous studies have demonstrated the biocompatibility and biodegradability of Mg-based materials, which have been employed for a wide range of orthopaedic applications, including nails, screws, splints, among others [7,27]. Materials formed from a matrix and reinforcements, commonly known as MMCs, are important to determine the mechanical characteristics of their base metals [8]. The biodegradable MMCs have exhibited biodegradable properties along with properties, such as tensile, yield strengths and Young's modulus. Additionally, metal reinforcement has improved the composite resistant to corrosion [9,29]. Mg-based implants are becoming more popular with bone tissue applications. In the grain boundary, Mg composites are prone to micro galvanic corrosion and electrochemical stratification. Powder metallurgy (PM) is used to manufacture Mg-based MMCs with high hardness, wear resistance and low thermal expansion coefficient for aerospace, defence and automobile applications [10]. As a biodegradable material, Mg and its alloys are increasingly recognized and highly attractive for medical treatments. They offer similar mechanical properties to bone tissue, provide functional functions within human bodies and are highly biocompatible. They also have a better strength to weight ratio than most other metallic and polymeric biomaterials [11,31]. The shapes and features of their composite provide strength to their mechanical and constructional properties, thereby resulting to a wide range of engineering applications. In addition to features, such as low density, peak specific strength and good stiffness with measurement strength, Mg composites also provide excellent patterns for the creation of more advanced remote sensing products. When they are compared with monolithic alloys, Mg composites have greater wear resistance. In order to make Mg and its alloys more durable, composites have been developed with hard and rigid reinforcement [12,15,32,34,35]. However, physiological environments rapidly corrode Mg, causing it to lose several mechanical properties [9].

Moving forward, zinc oxide (ZnO) also possesses a number of physical properties, making it appropriate for use as organic materials [13]. As an element native to the human body, Zinc (Zn) can be processed and released from the body through metabolism, which makes it an ideal alloying element for biocompatibility. Humans need Zn for the synthesis of more than 300 enzymes and it is involved with the activities of more than these enzymes. The body suffers from a Zn deficiency in which deoxyribonucleic acid (DNA) replication is slowed; thus, limiting protein synthesis [14,31,33]. As one of the most important members of the metal oxide family, ZnO is an important material in terms of its mechanical, electrical and optical properties [15,28]. In recent decades, ZnO has been a highly studied semiconductor material, due to its unique optical, magnetic and electrical properties. Various morphologies and sizes of ZnO have been used in pharmaceutical creams, powders and dental pastes. ZnO is the best possible candidate to dope transition metals and rare earth metals, used to improve the performance of ZnO devices and explore new applications. The use of ZnO for chemical additives has been demonstrated in various industries in addition to improving polymer properties [16]. Introducing a ZnO coating to the surface of whiskers during composite preparation produced an interfacial reaction, which built a strong interface for composites and provided an effective and feasible way to improve wettability [17].

Besides, powdered materials are pressed into a desired shape and then heated to fuse the powder together in a controlled atmosphere. PM is a constantly and rapidly changing technology, this includes a wide variety of metals and alloys, as well as a variety of shapes and sizes [18,30]. When compared with powder particles, PM has a higher level of production methods. As a result, it is considered to be a superior method for MMCs. The PM process involves blending of metal powders, compacting them and then sintering them at elevated temperatures. PM can be used to reduce the cost of manufacturing engineering components, as it is a proven and economical method. The use of PM in manufacturing increases the thermal conductivity, tribological behviour, seizure property and machinability property of products [19,20].

Yu et al. [1] reported that AZ91D composite reinforced with ternary Ti_2AlC MAX particles exhibited better properties than a composite reinforced with binary ceramic particles, such as TiC or ZnO. Witte et al. [5] described that the implants are temporarily required to provide mechanical support to the injured or pathological tissues during healing. Many authors have investigated Mg alloys as biodegradable biomaterials in recent years. Xie et al. [4] reviewed the metals and their alloy coatings were studied from the economic and utility perspectives. Turan et al. [8] investigated into the addition of carbon nanotubes (CNTs) to AZ31B Mg alloy, which influenced its properties. According to the results obtained, CNTs reduced corrosion resistance, because they formed galvanic cells with Mg. Bansal et al. [13] studied and considered Zn to be the most popular mineral in hard tissues. It is involved in numerous physiological functions of the immune system and aids cell growth in the AZ31 Mg alloy. It is also involved in numerous physiological functions of the immune system. Guan et al. [14] reported that addition of Zn to a matrix. The matrix became stronger through solution and aging strengthening. It also improved the electrical potential and corrosion resistance. Selvam et al. [15] investigated into ZnO nanoparticles reinforced Mg matrix composites by PM technique and observed an improved wear resistance with the ZnO-Mg composite.

Chaubey et al. [36] reported on the synthesis of Mg-7.4%Al bulk proposed composite, using hot pressing followed by hot extrusion process. The mechanical properties of the proposed composites were examined by using compressive strength. To examine the structure mechanism relation, the fracture surface after compression test was done to investigate the crack propagation implementation. Chaubey et al. [37] investigated into the microstructural development of the Mg-7.4%Al alloy by X-ray diffraction, scanning and transmission electron microscopies. Mg-7.4%Al powder was manufactured by using mechanical alloying with high-energy mill. The deviation of crystallite size and lattice strain were examined during milling process. Hardness of the powders was also evaluated as a function of milling time. Mg cores showed lower hardness of 40–50 HV and the Mg-Al combined regions displayed the higher hardness of 170 HV. Shadangi et al. [38] examined the PM process of AA 6082 Al matrix composite reinforced by non-equiatomic AlSiCrMnFeNiCu high-entropy alloy (HEA). The microstructure evolution and phase composition of Al-HEA powders were distinguished by scanning electron microscopy (SEM)/energy dispersive X-ray (EDX), X-ray diffraction (XRD) and transmission electron microscopy (TEM). Al-HEA nanocomposite powders were associated with the help of pressure-less sintering process at 560 °C. The microhardness of Al-HEA nanocomposites were measured in the series of ~ 0.90–1.81 GPa. The properties of the aluminium matrix composites (AMCs) can be personalized and improved by strengthening them with the suitable reinforcement particles. AMCs have presented an significant increase in HV, due to the uniform distribution of reinforcement particles and development of the transition layer at the boundary. Nandhini et al. [39] investigated into the equiatomic MgAlSiCrFe high-entropy alloy by using mechanical alloying process. The phase composition, phase evolution, alloying behavior and thermal strength of as-milled nanostructured powders of HEA were determined through XRD, TEM, SEM and differential scanning calorimetry (DSC). The nanocrystalline HEA powder was developed during milling with a crystallite size of 19 ± 0.8 nm. In the past three decades, significant efforts have been given to the growth of high-strength materials. This led to the innovation of quasicrystals, bulk metallic glasses and HEA. Shadangi et al. [40] studied the effect of Al–Cu–Fe (40 vol%) quasicrystalline (QC) reinforcement particle on the microstructure morphology and

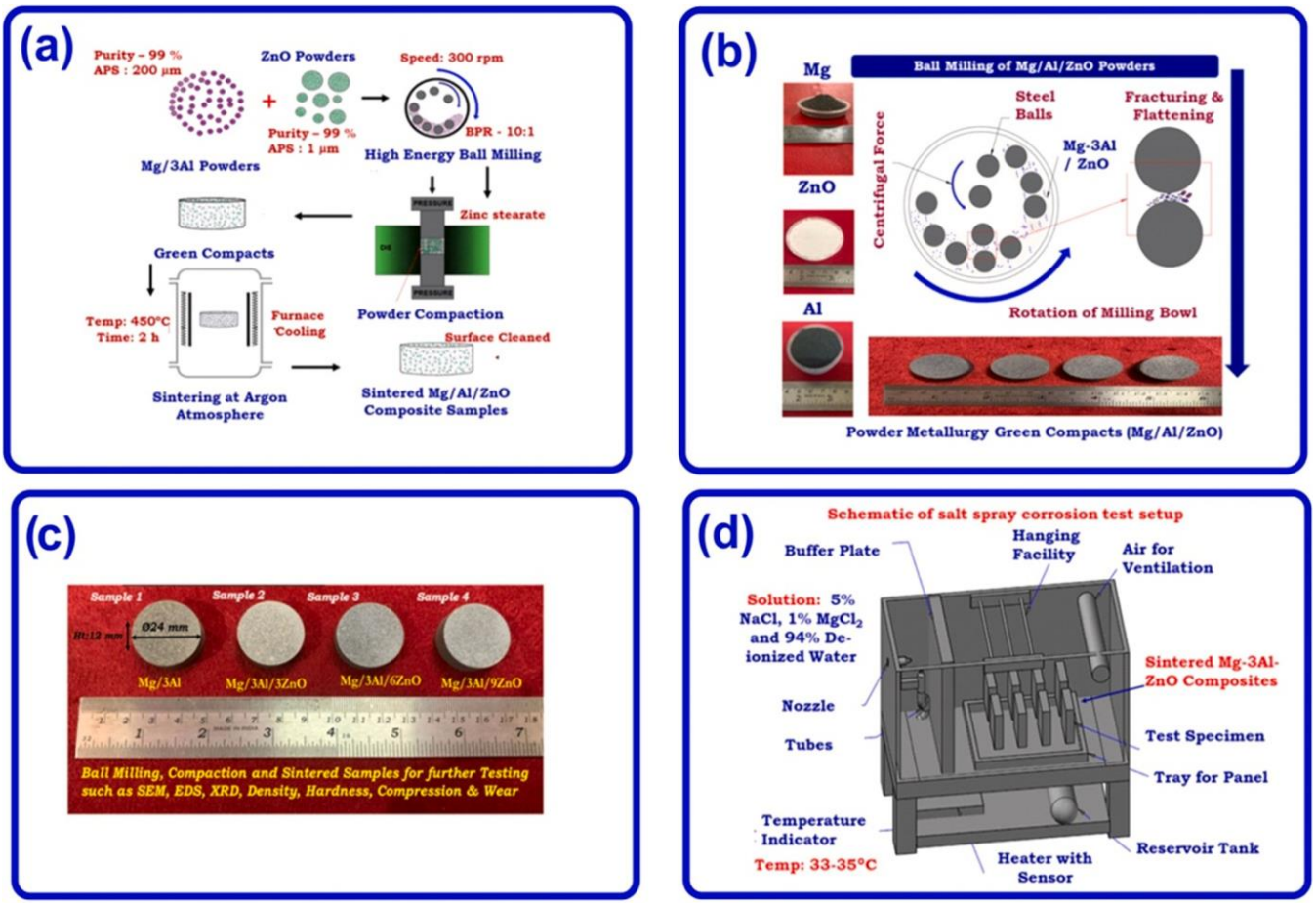

Fig. 1. (a) Schematic of PM process for Mg-3Al-ZnO composite, (b) images of Mg, Al and ZnO powders as well as the fabricated composite samples, (c) sintered samples of the various composites used and (d) schematic of salt spray corrosion test setup.

phase composition of AMCs manufactured by mechanical milling process and spark plasma sintering (SPS). The characterization of AMCs was analyzed through XRD, TEM and SEM. AMCs are conservatively strengthened with ceramic particle reinforcement, such as carbides, nitrides and oxides, having higher strength, modulus of elasticity and thermal stability.

Suguna et al. [41] analyzed the hexagonal phase ZnO nanostructures, using hydrothermal method with different temperatures: 200, 400, 600, 800 and 1000 °C. The XRD, Fourier Transform infrared spectroscopy (FTIR), field emission scanning electron microscopy (FE-SEM), high-resolution transmission electron microscopy (HR-TEM), ultra-violent-vis diffuse reflectance spectroscopy (UV-DRS) and X-ray photoelectron spectroscopy (XPS) techniques were characterized for the proposed nanostructures. The crystallite bulks of the proposed nanomaterials were measured by Williamson–Hall plots techniques. The ZnO strengthened at 200 °C displayed a crystallite size of 18.7 nm while the ZnO annealed at °C indicated a 46.2 nm. When increasing the annealing temperature, the crystallite sizes were improved, because of persuaded development of crystallites for the period of annealing procedure. Similarly, the band cracks of the ZnO annealed at different temperatures displayed a decreasing trend with increasing annealing temperatures. Prabhu et al. [42] manufactured the spindle-shaped ZnO and reduced graphene oxide sheets by using hydrothermal method. ZnO/r-GO composite was produced by direct solution mixing technique. Numerous characterization outcomes established the interior and exterior decoration of spindle-shaped ZnO on the reduced graphene oxide sheets. The surface states, optical properties, phase formation, morphology and crystalline structure were characterized by using UVeVis spectroscopy, TEM, XPS, FTIR, XRD and FESEM. Prabhu et al. [43] synthesized the well-defined dumbbell shaped ZnO by hydrothermal method and ZnO dumbbell/reduced graphene oxide (ZnO/rGO) nanocomposites were produced by a simple solution mixing method. The development of shape, nanocomposites, crystal structure, size and optical properties of the ZnO/rGO nanocomposites were examined by several analytical methods. Prabhu et al. [44] produced the djembe like ZnO microstructure evolution by surfactant-assisted hydrothermal method and the composite with g-C_3N_4 was manufactured by an ethanolic reflux method. In addition to electrical, optical, morphological and their photocatalytic activities were examined. The photocatalytic presentation was examined by dye degradation test under visible light irradiation. Jayakrishnan et al. [45] manufactured the dumbbell-shaped ZnO nanostructure, using hydrothermal method through elevated hydrothermal temperature of 200 °C. The XRD displayed the development of the hexagonal crystalline structure with high-phase purity. XPS was used to analyze the chemical surface states. The ZnO nanostructured materials exhibited possible applications, as super capacitors and textile wastewater treatments.

Considering the afore-reported extensive literature, it was evident that several manufacturing processes have been used to support the relevance of ZnO and other particles as reinforcements in Mg-based composites. Nevertheless, there was no reported study exactly on influences of ZnO addition on both microstructure and mechanical properties of sintered Mg matrix composites, specifically with variable ZnO filler contents of 0–9 wt percentage (wt%) and PM technique. The main objective of this study was to synthesize Mg- 3Al-xZnO (where x = 3, 6 and 9 wt%). Therefore, the present work

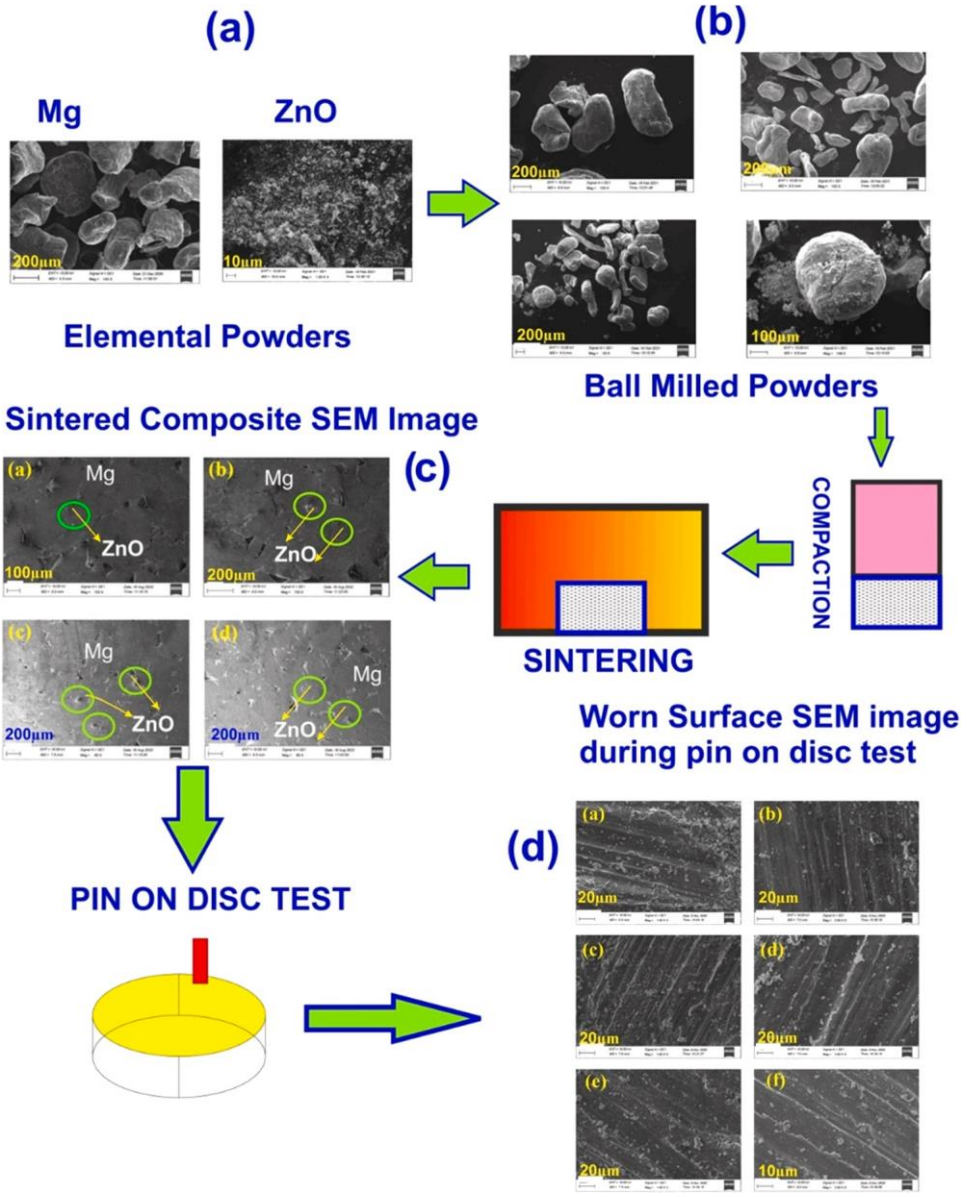

Fig. 2. (a) SEM images of as-received Mg and ZnO powders, 2 (b) SEM images of ball milled Mg-3Al-ZnO composite powders, showing (a) Mg-3 wt%Al-3 wt%ZnO, (b) Mg-3 wt%Al-6 wt%ZnO, (c) & (d) Mg-3 wt%Al-9 wt%ZnO. 2 (c) SEM images of sintered Mg-3Al-ZnO composites, showing (a, b) Mg-3 wt%Al-3 wt%ZnO, (c) Mg-3 wt%Al-6 wt%ZnO and (d) Mg-3 wt%Al-9 wt%ZnO. 2 (d) Worn surface images of sintered Mg-3Al-ZnO composites, showing (a, b) Mg-3 wt%Al-3 wt%ZnO, (c, d) Mg-3 wt%Al-6 wt%ZnO and (e, f) Mg-3 wt%Al-9 wt %ZnO.

studied various Mg-3Al-ZnO composite samples, which were manufactured through PM technique. The microstructure, mechanical and corrosion properties of the proposed composites were analysed. The worn surfaces of the samples were thoroughly studied, using scanning electron microscopy (SEM). The suitable wear parameters were identified, based on signal-to-noise (S/N) ratio analysis. The contour and probability plots were provided for better understanding of the influences of wear parameters on their wear rate (W*R*) and coefficient of friction (COF). The optimal process parameters were obtained for the best composite sample.

2. Experimental details

Fig. 1(a) depicts the PM process used to fabricate the Mg-3 wt %Al-ZnO composites. Fig. 1(b-d) show the images of Mg, Al and ZnO powders used in this work and fabricated composite samples: Mg-3 wt%Al, Mg-3 wt%Al-3 wt%ZnO, Mg-3 wt%Al-6 wt%ZnO and Mg-3 wt%Al-9 wt%ZnO. The powders were received from Kemphasol, Mumbai, India. The Mg powders were 99% pure and possessed a particle size of < 200 µm. To prepare the composite mixtures, certain measured amounts of powder were ball milled in a planetary mill at a speed of 120 rpm for 3 h with the ball-to-powder ratio of 10:1.

The ball milled powders were compacted, using a hydraulic press (Model: Universal Tun-400) with height of 12 mm and diameter of 24 mm. Zinc stearate was used as a binder to ease compact ejection. Green compacts were sintered in a high temperature. Argon furnace (Model: Hi-Tech 1200 °C) with a vacuum pump was used for 2 h at 450 °C at a rate of 10 °C/min to complete the compacting process. Magnesium melted around 650 ºC. During powder metallurgy process, sintering temperature was considered as 60–70% of the melting point of the alloy. Therefore, 450 ºC was between the sintering range, where the process was carried out for 2 h. Azaath et al. [48] synthesized PM copper –SiC composites in argon atmosphere tubular furnace, where the hold or soaking period was only 30 min, which was much less than the present investigation. Samples were cooled in the furnace during the sintering process. The sintered composites

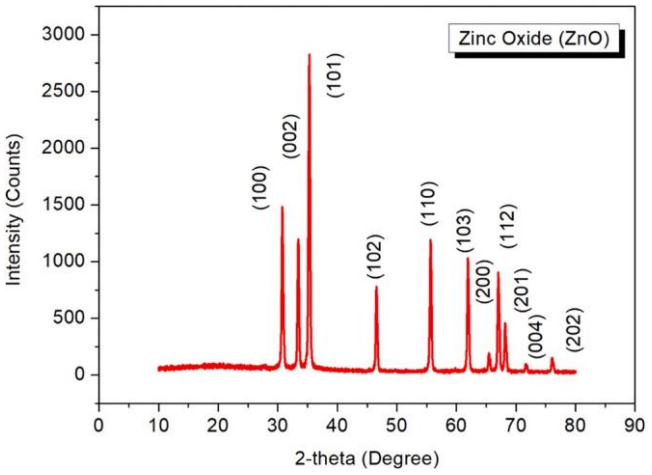

Fig. 3. XRD pattern of ZnO powder.

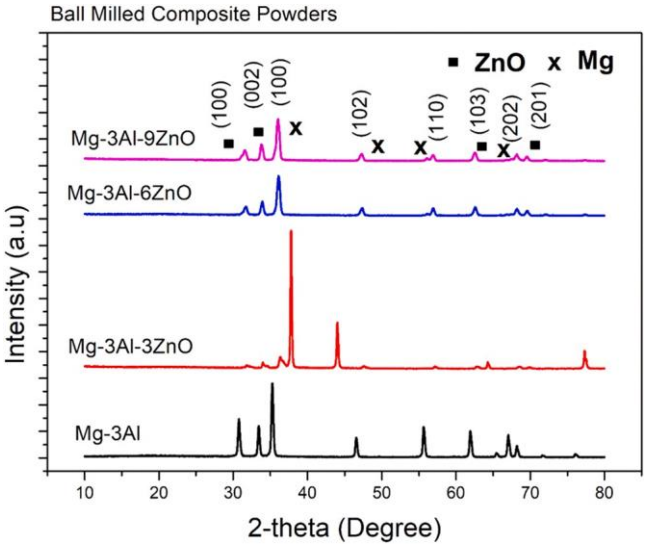

Fig. 4. XRD patterns for Mg-3 wt%Al-ZnO composite powders.

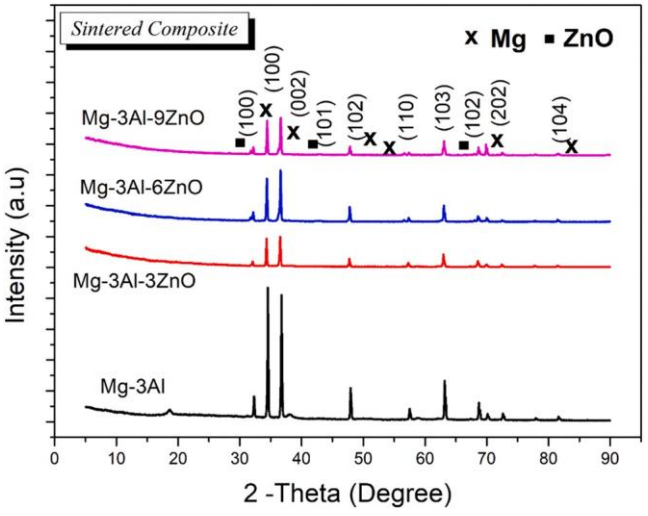

Fig. 5. XRD patterns for Mg-3Al-ZnO sintered composite samples.

Table 1
Parameters and levels.

wt% of ZnO	0	3	6	9
Applied load, P (N)	5	10	15	20
Sliding distance, D (m)	500	1000	1500	2000
Sliding velocity, V (m/s)	1	2	3	4

were cleaned with emery sheets and then polished with a polishing machine before testing. Fig. 1(c) shows the sintered samples of Mg-3 wt%Al, Mg-3 wt%Al-3 wt%ZnO, Mg-3 wt%Al-6 wt%ZnO and Mg-3 wt %Al-9 wt%ZnO.

By employing Archimedes' principle, the densities of the Mg-3 wt % Al alloy and its composites were determined [46]. Based on the Archimedes' principle, a density measuring kit was used to calculate the density of the sample. The rule of mixture was used to calculate the theoretical density, experimental density and % of porosity. A weighing balance with a precision of 0.0001 g was used to record the weights of each sample. This method was adopted based on the previous investigation on synthesis of Mg-3 wt%Al-ZnO composites and Mg-3 wt%Al samples [49].

In this study, the theoretical densities of the ball-milled Mg alloy and its composites were calculated, using the densities of Mg, Al and ZnO. In addition, SEM (Make-EVO-18, Carl Zeiss) and energy dispersive spectroscopy (EDS) (Make-TESCAN VEGA3-Wsource) were used for the evaluation of the morphology of the ball milled Mg alloy and its composites. The proposed composites were analyzed, using SEM for composition and microstructure. Fig. 2(b) shows the SEM images of the Mg and ZnO. X-ray diffraction (XRD) measurements were carried out, using Malvern Panalytical X Pert³Powder System with a Cu-K α (λ = 1.54060 A°) operated at 20 mA and 40 kV for ball

Table 2
Experimental details.

Exp. Number	wt% of ZnO	P (N)	D (m)	V (m/s)	WR (mm³/m)	COF	S/N ratio WR	Mean WR	S/N ratio COF	Mean COF
1	0	5	500	1	5.861	0.55	-15.3594	5.861	5.192746	0.55
2	0	10	1000	2	6.247	0.52	-15.9134	6.247	5.679933	0.52
3	0	15	1500	3	7.864	0.56	-17.9129	7.864	5.036239	0.56
4	0	20	2000	4	11.697	0.63	-21.3615	11.697	4.013189	0.63
5	3	5	1000	3	5.247	0.30	-14.3982	5.247	10.45757	0.30
6	3	10	500	4	6.278	0.46	-15.9564	6.278	6.744843	0.46
7	3	15	2000	1	6.957	0.50	-16.8484	6.957	6.020600	0.50
8	3	20	1500	2	9.361	0.61	-19.4264	9.361	4.293403	0.61
9	6	5	1500	4	6.934	0.44	-16.8197	6.934	7.130946	0.44
10	6	10	2000	3	7.348	0.49	-17.3234	7.348	6.196078	0.49
11	6	15	500	2	7.869	0.52	-17.9184	7.869	5.679933	0.52
12	6	20	1000	1	8.624	0.59	-18.7142	8.624	4.582960	0.59
13	9	5	2000	2	3.215	0.39	-10.1436	3.215	8.178708	0.39
14	9	10	1500	1	3.694	0.41	-11.3499	3.694	7.744323	0.41
15	9	15	1000	4	3.785	0.46	-11.5613	3.785	6.744843	0.46
16	9	20	500	3	4.128	0.48	-12.3148	4.128	6.375175	0.48

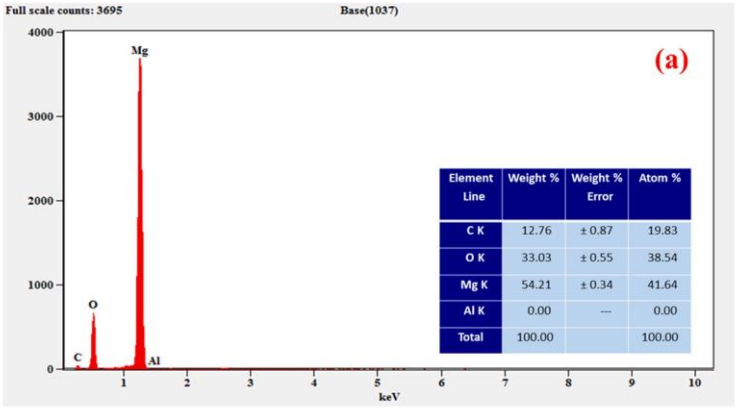

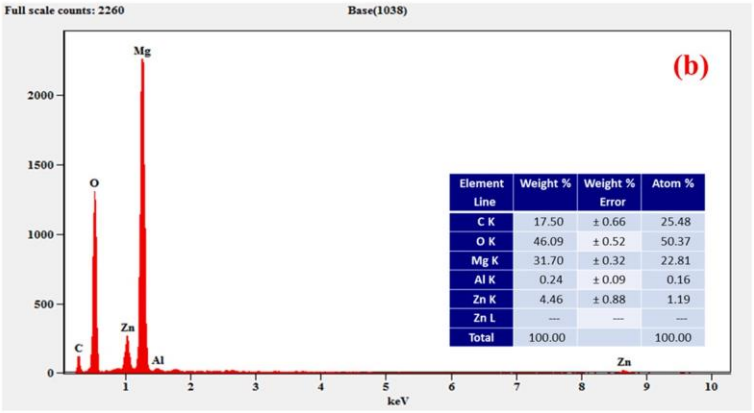

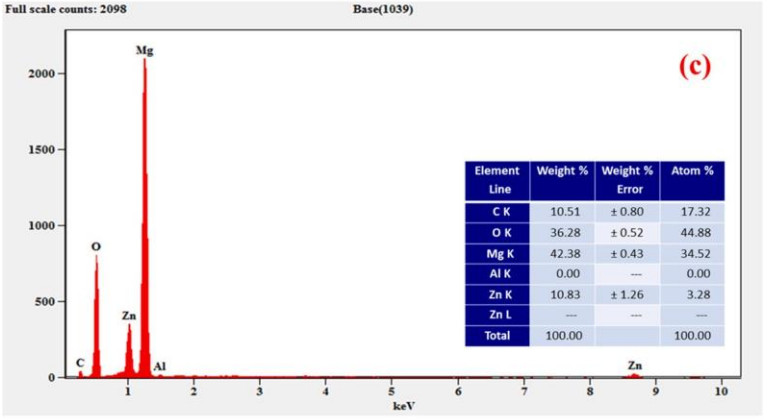

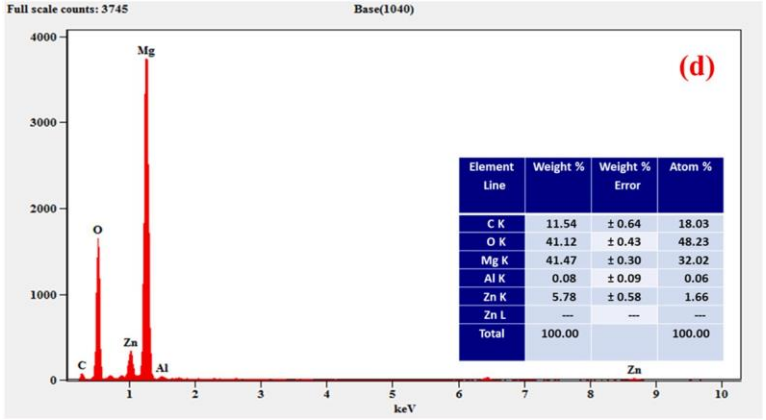

Fig. 6. EDX of sintered Mg-3Al-ZnO composites (a) Mg-3 wt%Al-0 wt%ZnO (b) Mg-3 wt%Al-3 wt%ZnO, (c) Mg-3 wt%Al-6 wt%ZnO and (d) Mg-3 wt%Al-9 wt%ZnO.

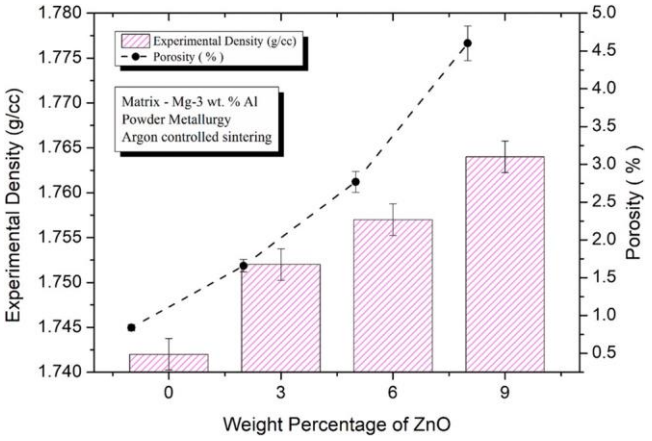

Fig. 7. Effects of ZnO on the densities of the various samples.

milled composite powders and sintered composite samples. Fig. 3 depicts the XRD pattern of as-received ZnO powder. The XRD patterns of Mg-3Al powders were reported in our previous publication [47]. Al powder XRD was not provided, due to the presence a matrix with a lower weight percentage of 3, the Al peak was not apparent in the XRD pattern. The integration of low weight percentages of reinforcement elements. Generally, if the presence of any element is less than 5 wt%, it cannot be detected by XRD [54].

Hardness tests were conducted on sintered composite samples according to the E-384 ASTM standard with an automatic digital micro hardness tester (Model: Holmarc MV1-PC) under 1 Kg of load and 15 s of dwell time. An average value was taken for the hardness based on the results obtained from five locations on each of the samples. More also, the compressive strengths (CS) of the sintered composites were determined in accordance with ASTM E-9 standard, using an ASTM-approved universal testing machine (Model: M-50) with a 50 kN capacity and crosshead speed of 3 mm/min.

In accordance with ASTM B-117 (corrosion tests under artificial atmospheres - salt spray tests), corrosion tests were conducted using salt spray. A 5% sodium chloride, 1% magnesium chloride and 94% de-ionized water solution with temperature of 33–35 °C and relative humidity of 98% were used in 1.0 litre of solution at relative humidity of 98%. Each sample was weighed after eight hours, a buffer solution was added and a pH of 7.5 maintained. Fig. 1(d) shows the schematic of salt spray corrosion test setup. Continuous air was

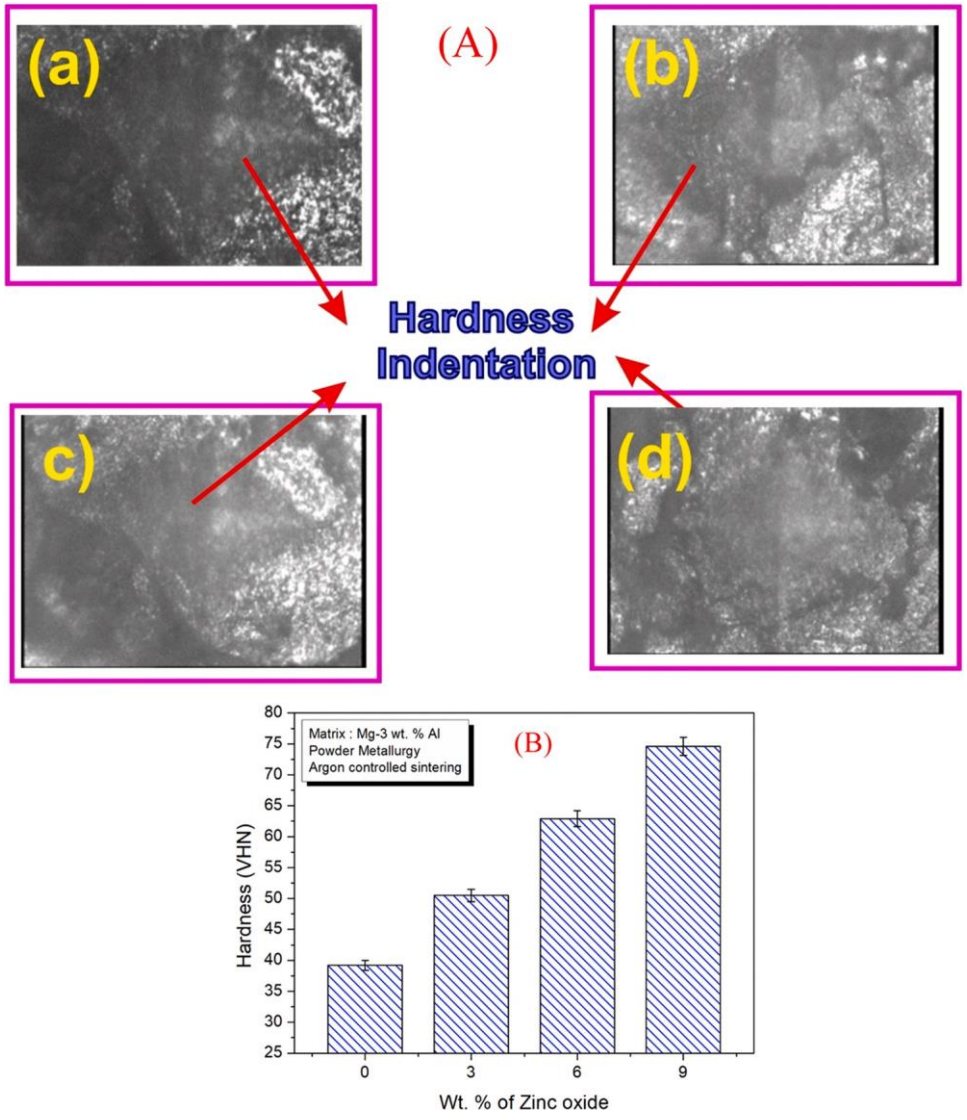

Fig. 8. (A) Indentation marks: (a) Mg-3 wt%Al, (b) Mg-3 wt%Al-3 wt% ZnO, (c) Mg-3 wt%Al-6 wt% ZnO, (d) Mg-3 wt%Al-9 wt% ZnO and (B) effects of ZnO on the hardness values of the various samples.

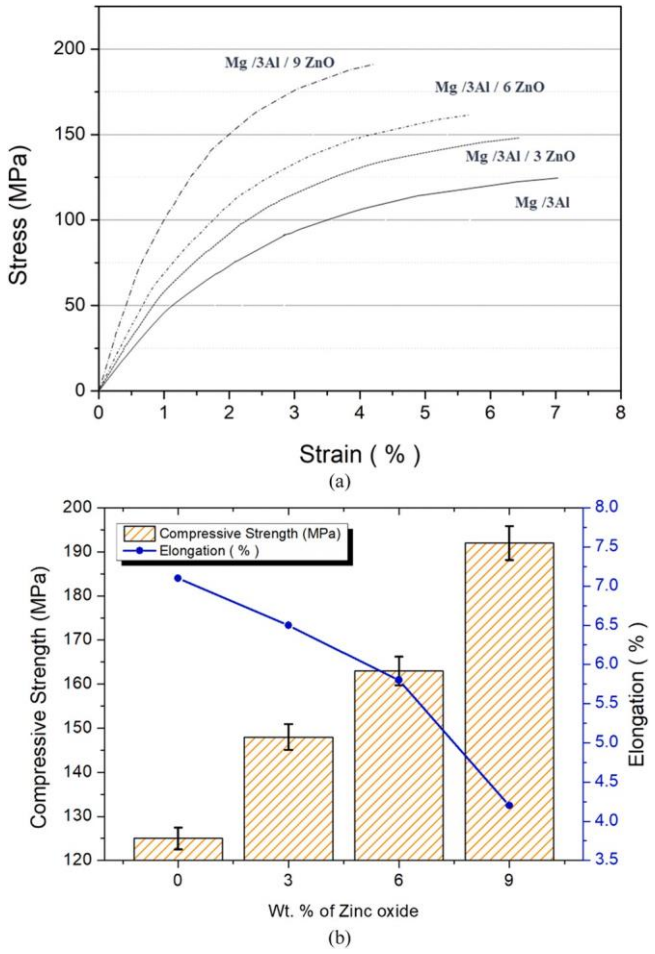

Fig. 9. (a) Stress/strain plots and (b) effects of ZnO on the CS and elongations of the various samples.

atomized at 2–3 bars, using pressure regulation. Following each weight measurement, the corrosion rate was calculated on the horizontal surface area of the experiments, which was 12 cm^2. The experiment was tilted at 45° to the plumb line.

Furthermore, pin-on-disc setup (Make: Ducom Wear test) was used to determine their wear rate (W*R*) and coefficient of friction (COF). The pin-on-disc test involved inserting an elbow-shaped pin perpendicularly into the circular counter plate. By using a lever and weight, the specimen was pressed against a rotating disc at a given load. The disc was also rotated at a specified speed. The quantity of wear was determined by weighing the pin before and after the test. During this experiment, specimens with a diameter of 10 mm and a length of 30 mm was used, as similarly reported [21]. Test was conducted according to the ASTM G99 standard. The thickness and diameter of the hardened steel disc were 8 and 165 mm, respectively. Weight difference method was used to determine loss of wear. The friction force was measured with friction sensors. The friction coefficients were later calculated by measuring the friction force. The experimental design used was based on Taguchi L_{16} orthogonal array, as similarly employed [24]. Detailed information on parameters, levels and experimental details are presented in Tables 1 and 2. Both Eqs. (1) and (2) were used to determine the value of W*R*.

$$WR = \frac{Mass\ \ loss\ \ x\ \ Density}{D}(mm^3/m) \quad (1)$$

$$V = \frac{\pi DN}{1000} \quad (2)$$

Eq. (2) Where V = Velocity (m/min), D = diameter (mm) and N= speed (rpm).

3. Results and discussion

3.1. Characterization analysis of composite powders

Previously, Fig. 2(b) depicts the SEM images of ball milled Mg-3Al-ZnO composite powders. The ZnO particles were evenly distributed within the Mg alloy matrix. As observed, the ZnO particles were not agglomerated in the Mg alloy matrix. This can be attributed to proper powder milling process. The presence of more ZnO content was observed in Fig. 7(c) and (d) for the Mg-3 wt%Al-9 wt%ZnO composite sample. According to the SEM analysis, the ZnO powders were smaller than the matrix particles of Mg. The compaction process was followed after ball milling process. The ZnO powder size was reduced after ball milling process. The size of ZnO was lower than size of Mg, therefore ZnO entrapped between the spaces of Mg during the compaction process. Reinforcing particles were also measured by their size and shape to determine the required properties of the composites [15,23].

The planes of both matrix and reinforcement can be observed by examining the XRD patterns. Therefore, Fig. 4 shows the XRD patterns obtained from the milled Mg-3 wt%Al-ZnO powders. Mg recorded the higher peak in all of the patterns and ZnO produced the lower peak, because ZnO was at a lower concentration than Mg. Adding ZnO to the Mg-3 wt% Al alloy matrix reduced the peak intensity of Mg in the composite. ZnO was well incorporated into the Mg matrix, as evident from the XRD patterns of the composite powders. Additionally, it was significantly observed that there were no other compounds formed in the high energy ball milling process, similar to the earlier reported results. ZnO peak of XRD patterns were recognized and indexed based on reported patterns: JCPDS No. 36–1451. The 2θ plotting is merely practical, because many machines use fixed sources, which results to a measured detector angle of 2θ with respect to the incident beam. As the detection circuit typically counts the number of pulses (related to the number of detected photons), "counts" is the most widely used unit of measurement. Of course, choosing time at arbitrarily and graphing it in "counts" would not give an absolute scaling.

More also, Fig. 5 shows the XRD patterns obtained from the Mg-3 wt%Al alloy and Mg-3 wt%Al-ZnO composites sintered at 450 °C. There were many peaks recorded in all compositions of the synthesised composites, corresponding to Mg. The peak formed at 36 degrees adjoining to Mg peak was confirmed as ZnO. The Al peak in the XRD structure appeared to be less noticeable, because of its low content of 3 wt% used in the matrix.

The SEM images of the sintered Mg-3Al-ZnO composites have been previously shown in Fig. 2(c). Among all the images obtained, the ZnO particle was evenly distributed across the matrix. There was a better adhesion between the ZnO particle and Mg matrix, as observed from all the samples. There was no agglomeration observed on the samples with more wt% of ZnO. Due to the ball milling process, a uniform distribution was achieved among Mg, Al and ZnO powders. During the milling process, the size of ZnO was reduced, because the milling process was effective. Fracture of reinforcement was caused by the impact of the balls and particles on the reinforcements during milling operation [22].

Fig. 6(a)-(d) show the energy dispersive X-ray (EDX) images of Mg-3 wt%Al alloy and its ZnO reinforced composites. Fig. 6(a) depicts the Mg-3 wt% Al alloy, the Mg peak was significantly observed from the plot. Fig. 6(b)-(d) show the EDX of the composite samples and their respective ZnO and Mg peaks. Al peak was observed in Fig. 6(b) and (d), and weight and atomic percentages are provided in all the images. During the sintering process and at the same instance, vacuum was applied before the sintering. Therefore, oxide formation

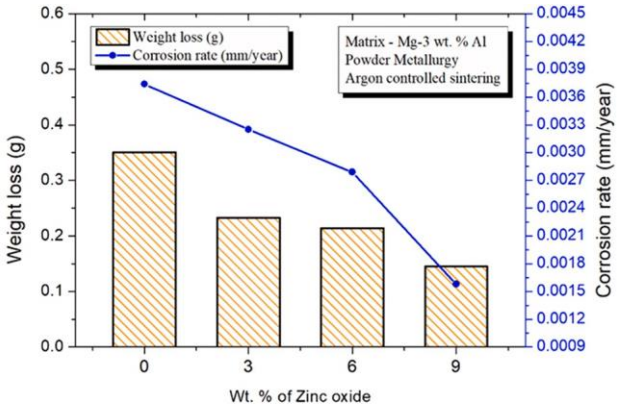

(a)

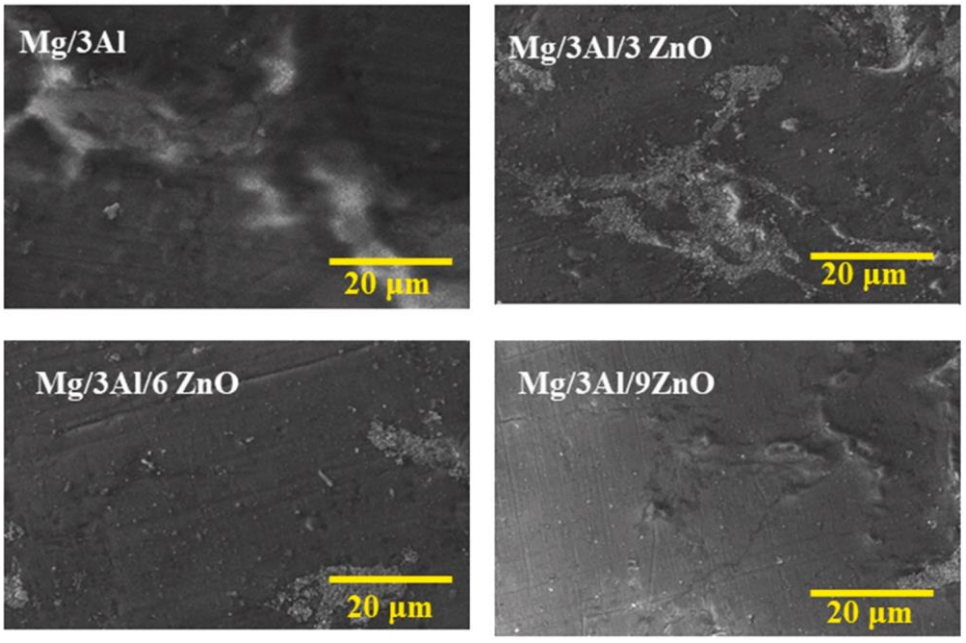

(b)

Fig. 10. (a) Effects of ZnO on the corrosion behaviors of the various samples and (b) corroded SEM images of Mg/3Al alloy and Mg/3Al/ZnO composites.

during sintering was very small. The same phenomena of presence of oxygen has been previously observed and reported in EDS results of synthesised Ni-10Co-5Cr, using PM [52].

Fig. 7 shows the effects of ZnO inclusion on the densities of Mg-3Al-ZnO composites. The density of the experimental sample increased with wt% of ZnO in Mg alloy matrix. Each sample has a theoretical density that was greater than the experimental density. Similarly, the porosity of the sample increased with the ZnO content in the matrix of Mg-3 wt%Al. Particles were effectively bonded together and voids were eliminated during the sintering process, which resulted to a higher density of sintered samples. Consequently, the sintered samples were denser than the green composite samples. The moisture from the samples was also removed during the heating process. The theoretical density is defined as the ratio of mass of sintered compact to the volume of the sintered compact. The experimental density is the density of sintered specimen which has low pore formation. The density of ZnO was higher than the density of magnesium, therefore the density increased with an increase in inclusion of ZnO. Due to the diffusion, sintered sample possess was higher density than green compact density. Eq. (3) was used for the porosity calculation.

$$Porosity = \frac{[(\rho_{Theoretical} - \rho_{Experimental})]}{\rho_{Theoretical}} \; x100 \quad (3)$$

Fig. 8(A) depicts the indentation marks on (a) Mg-3 wt%Al, (b) Mg-3 wt%Al-3 wt% ZnO, (c) Mg-3 wt%Al-6 wt% ZnO, (d) Mg-3 wt%Al- 9 wt% ZnO and Fig. 8(B) shows the influence of ZnO particle on the hardness property of Mg-3 wt%Al alloy matrix. By carefully examining the bar graph, it can be observed that the addition of ZnO to the Mg-3 wt% Al alloyed matrix increased the hardness of the composite material. The hardness of ZnO particles was higher than the base Mg matrix. Therefore, it was easier to improve its hardness when a hard and suitable particle was added to a soft Mg matrix. Composites with ZnO content of 9 wt% recorded the highest hardness, whereas base matrix alloys recorded the lowest hardness. It depends on many factors to achieve increased hardness, such as refined microstructures, the presence of secondary particles and uniform distribution of secondary particles. Those samples of Mg with over 9 wt% of ZnO produced poor mechanical property, hence they were not reported. In addition, the results were ranged downward, due to the increased reinforcement of ZnO. Therefore,

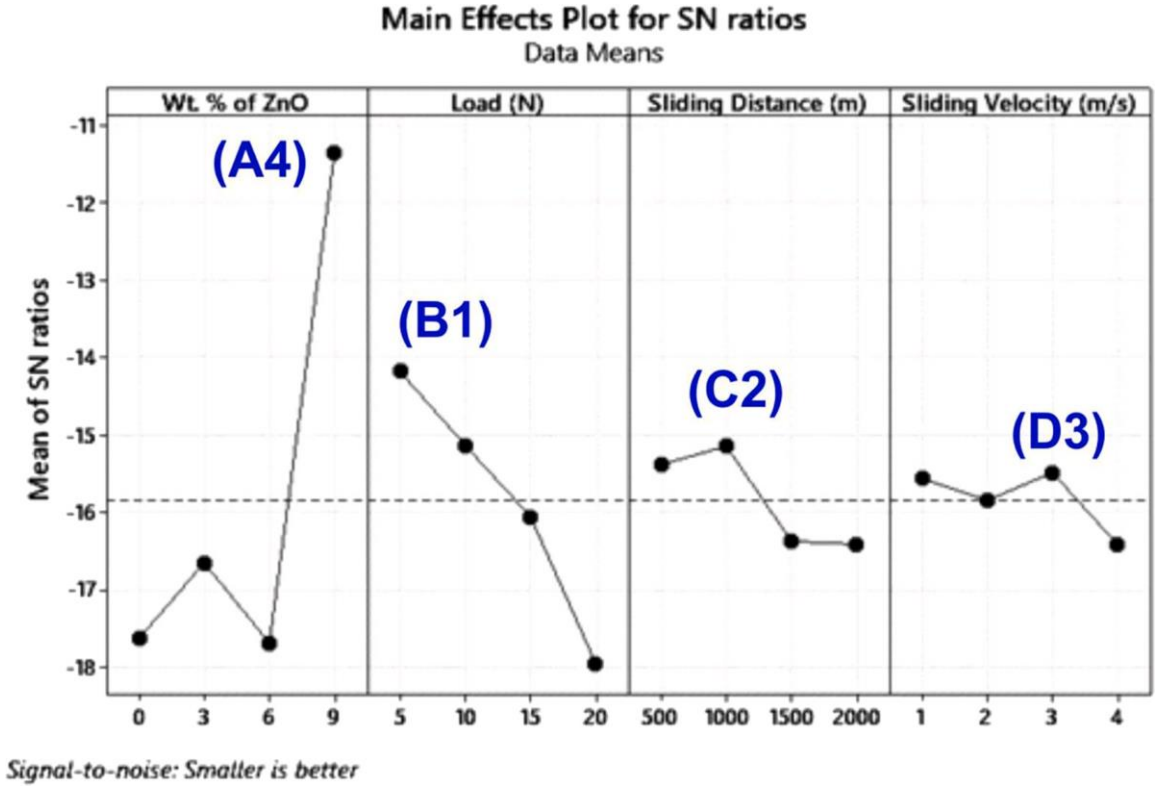

Fig. 11. S/N ratio plot of W*R* obtained from the Taguchi analysis for various input parameters wt% of ZnO, L, D and V.

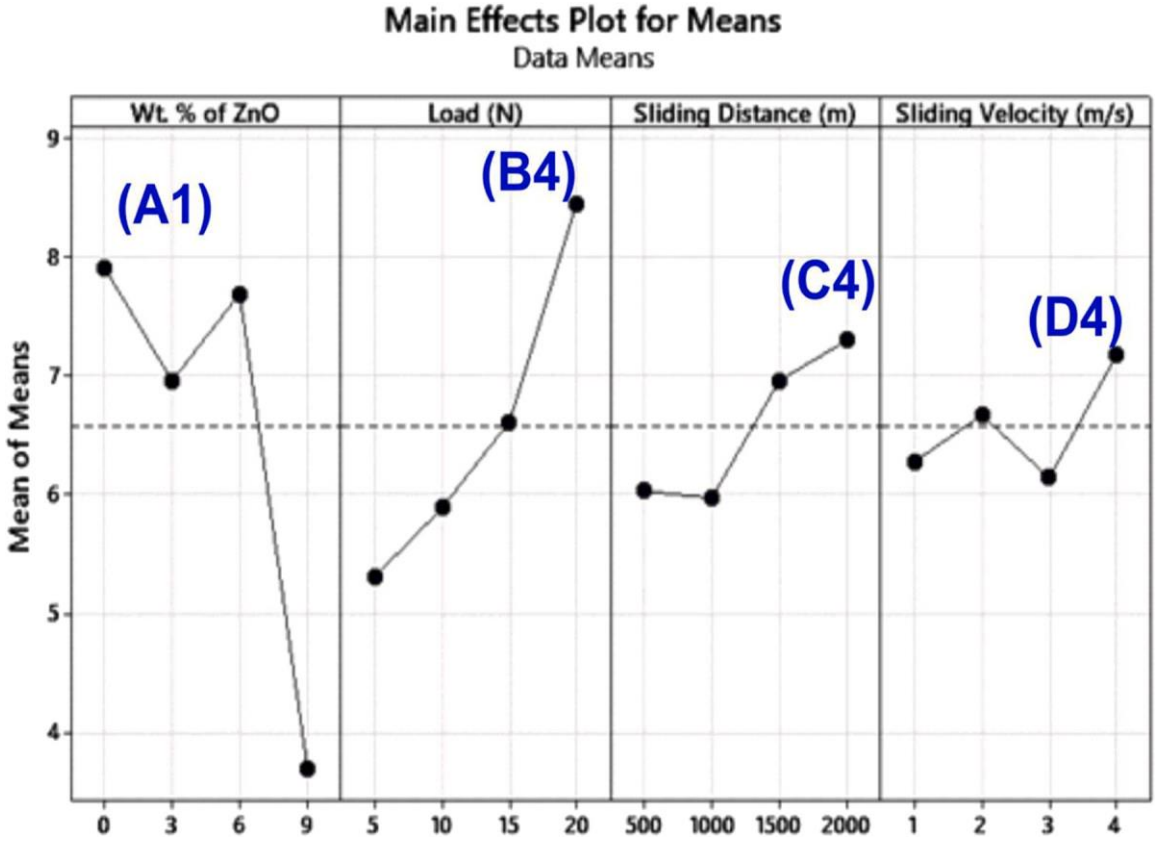

Fig. 12. Means plot of W*R* obtained from the Taguchi analysis for various input parameters wt% of ZnO, L, D and V.

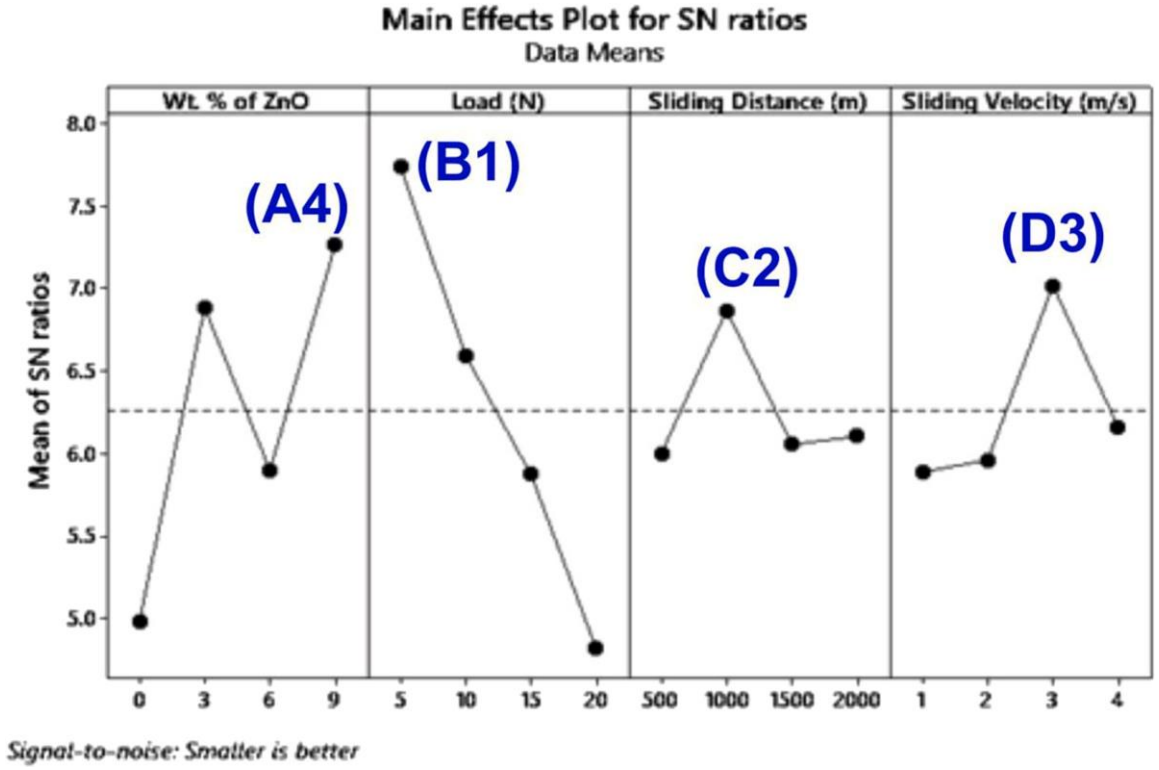

Fig. 13. S/N ratio plot of COF obtained from the Taguchi analysis for various input parameters wt% of ZnO, L, D and V.

the threshold value of ZnO was 9 wt% and it is not advisable to increase it more than this value.

Fig. 9(a) shows the stress/strain plots obtained for the samples tested under compression load. Fig. 9(b) depicts the CS and elongation of the Mg-3 wt%Al and Mg-3Al-ZnO composites. A higher CS resulted from an increasing ZnO content in the matrix of Mg-3 wt %Al. Another possible explanation is the decreased elongation of the composite sample, as a result of the presence of rigid particles in the

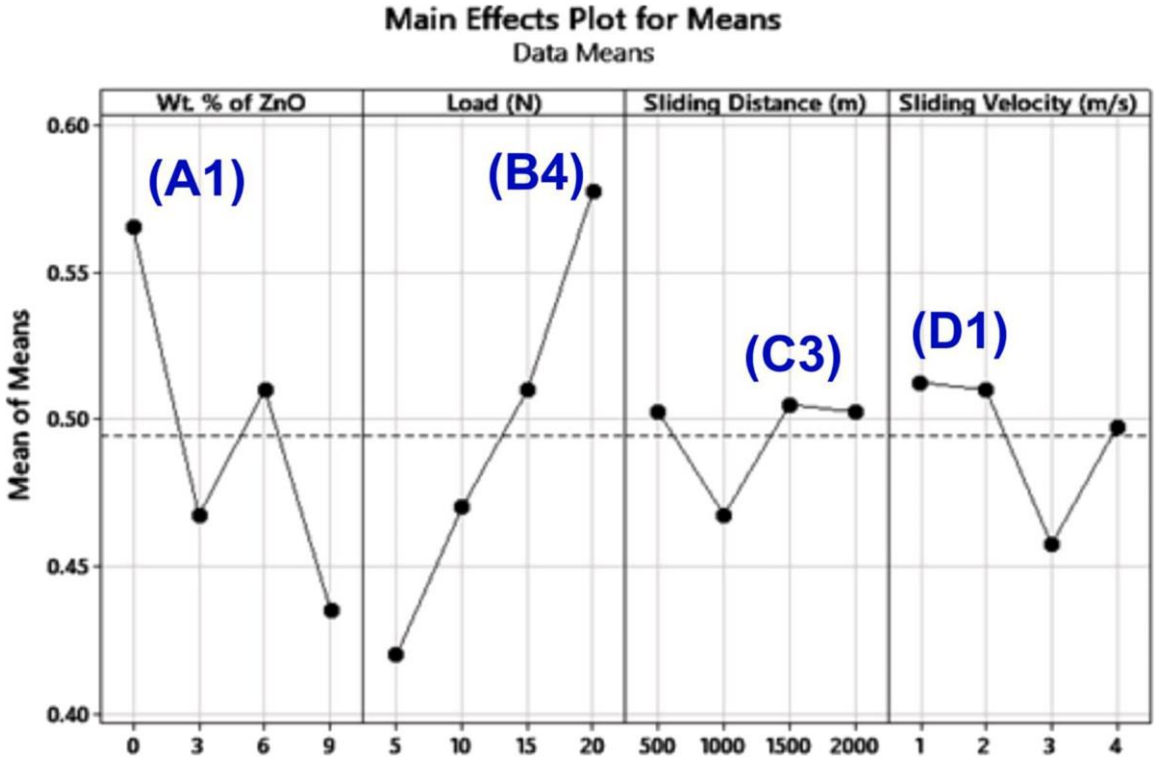

Fig. 14. Means plot of COF obtained from the Taguchi analysis for various input parameters wt% of ZnO, L, D and V.

Table 3
Response table for S/N ratios for W*R*.

Level	wt% of ZnO	P (N)	D (m)	V (m/s)
I	-17.64	-14.18	-15.39	-15.57
II	-16.66	-15.14	-15.15	-15.85
III	-17.69	-16.06	-16.38	-15.49
IV	-11.34	-17.95	-16.42	-16.42
Delta	6.35	3.77	1.27	0.94
Rank	1	2	3	4

Table 4
Response table for Means for W*R*.

Level	wt% of ZnO	P (N)	D (m)	V (m/s)
I	7.917	5.314	6.034	6.284
II	6.961	5.892	5.976	6.673
III	7.694	6.619	6.963	6.147
IV	3.705	8.453	7.304	7.173
Delta	4.212	3.138	1.328	1.027
Rank	1	2	3	4

Table 5
Response table for S/N ratios for COF.

Level	wt% of ZnO	P (N)	V (m/s)	D (m)
I	4.981	7.740	5.998	5.885
II	6.879	6.591	6.866	5.958
III	5.897	5.870	6.051	7.016
IV	7.261	4.816	6.102	6.158
Delta	2.280	2.924	0.868	1.131
Rank	2	1	4	3

Table 6
Response table for Means for COF.

Level	wt% of ZnO	P (N)	V (m/s)	D (m)
I	0.5650	0.4200	0.5025	0.5125
II	0.4675	0.4700	0.4675	0.5100
III	0.5100	0.5100	0.5050	0.4575
IV	0.4350	0.5775	0.5025	0.4975
Delta	0.1300	0.1575	0.0375	0.0550
Rank	2	1	4	3

Mg-3 wt%Al matrix. As a result, the ductility decreased and the hardness of the composite increased. In order to improve the CS, ZnO particles in the matrix must be evenly distributed and properly bonded with the Mg matrix. CS was highest in the Mg-3 wt%Al-9 wt% ZnO composite sample, while the Mg-3 wt%Al alloy sample recorded a relatively low CS. The ZnO peak ensured a stable connection between Mg and ZnO. The strength of the composite was increased by incorporating ZnO to the matrix. It was observed that ductility decreased when ZnO content was increased. This can be attributed to the following reasons: (i) irregular interfacial bonding strength in the middle of the fillers and matrix material and (ii) irregular allotment of fillers with matrix and poor plasticity. Therefore, there was a decrease in elongation, similar to a previous study [53].

Fig. 10(a) shows the effects of ZnO on the corrosion behaviors of the various samples. The corrosion rate (mm/year) and weight loss of the Mg-3 wt%Al alloy and Mg-3Al-ZnO composite are presented in Fig. 10. According to the plot, the addition of ZnO to the Mg-3 wt%Al alloy in the salt spray test reduced the weight loss. Consequently, the corrosion rate (mm/year) also decreased with an increase in the amount of ZnO in Mg-3 wt%Al matrix. This indicated an improved corrosion resistance in the composites [14]. In this case, ZnO was spread appropriately in the grain boundary of the matrix. It also created a passive layer of protection for the surface against corrosion. Mg-based alloys are very relevant to biomedical applications. However, it is prone to corrosion in the presence of chloride ion. When oxide particle was added to the matrix, the corrosion resistance of the Mg alloy was enhanced. Therefore, heterogeneous microstructure of the composite contributed to its enhanced corrosion resistance [19]. The low corrosion rate observed from the samples with 9 wt% of ZnO was 0.00158 mm/year, while Mg-3 wt%Al alloy exhibited the higher corrosion rate of 0.00374 mm/year. Fig. 10(b) depicts the corroded SEM images of Mg/3Al alloy and Mg/3Al/ZnO composites. The corroded surface evidently showed that the composite samples exhibited less corroded spots, when compared with unreinforced Mg/3Al alloy sample.

3.2. Analysis of variance

Analysis of variance (ANOVA) was used to analyze the effects of parameter combinations on the responses. A significance level of 5%; 95% confidence level was used for the response optimization study [22,23]. The COF values increased when the loading was high and the sliding speed was low. Localized welding on the sliding surfaces was responsible for the higher COF values. COF values were higher for sliding surfaces when loaded more, as they are more localized [24].

3.2.1. S/N ratio of analysis

Figs. 11 and 12 depict S/N ratio and the mean plots for the W*R*, respectively.

For the most W*R*, it was observed that the reinforcement levels of $A_4B_1C_2D_3$ were better at Level IV (9 wt%), P at Level I (5 N), D at Level II (1000 m) and V at Level III (3 m/s). Fig. 13 shows the S/N ratio plot of COF. Fig. 14 depicts the mean plot for the COF. From the analysis, it was evident that the combined parameters of $A_4B_1C_2D_3$ produced the optimum COF. It represented the reinforcement at Level IV (9 wt %), P for level I (5 N), D for level II (1000 m) and V for level III (3 m/s).

Moving forward, Tables 3–6 present the S/N ratios and Mean values for the W*R* and COF, respectively. Reinforced alloys experienced varying WRs, depending on the applied load. W*R* varied significantly in response to the applied load. According to Archard's law, which states that wear between surfaces is proportional to the normal pressure or load applied. This implies that when a load is applied, W*R* changes in proportion to the load. Therefore, the composite samples recorded a lower W*R* than alloy reinforced with Mg-3Al-ZnO, due to an increasing applied loads. With metal matrix reinforcements, wear coefficients decreased and volumetric losses reduced, since metal matrix particles were present. Mg-3Al particles reduced the rate of material removal, thereby increased the hardness of the composites at the same time. With low loads, W*R* was low, because the surface interacting pressure was lower as well as the existence of self-lubricating ZnO particles. W*R* was lower at low loads, because ZnO particles were self-lubricating and the surface interacting pressure was lower. Consequently, the rates of material removal from reinforced alloy were higher, because the surface debris adhered to the particles. It later resulted to a greater material removal, due to the high pressures developed at the interface of the alloys [21,25,26].

3.2.2. Contour plot analysis

Fig. 15(a)-(f) show the contour plots for W*R*. The plots of W*R* *versus* P and wt% of ZnO are shown in Fig. 15(a). It can be observed from the green plot that the reduction in W*R* was related to the increase in ZnO wt% in the right corner. With regards to the P and D, plots 15(a)-(f) follow the same pattern. From Fig. 15(a), the dotted red line indicated the interaction between reinforcement and ZnO wt% and D, and how it increased the W*R*. The plot also demonstrated how two parameters interacted for W*R*. Similarly, Fig. 16(a)-(f) depict the contour plots for COF, including the plots for P *versus* wt% of

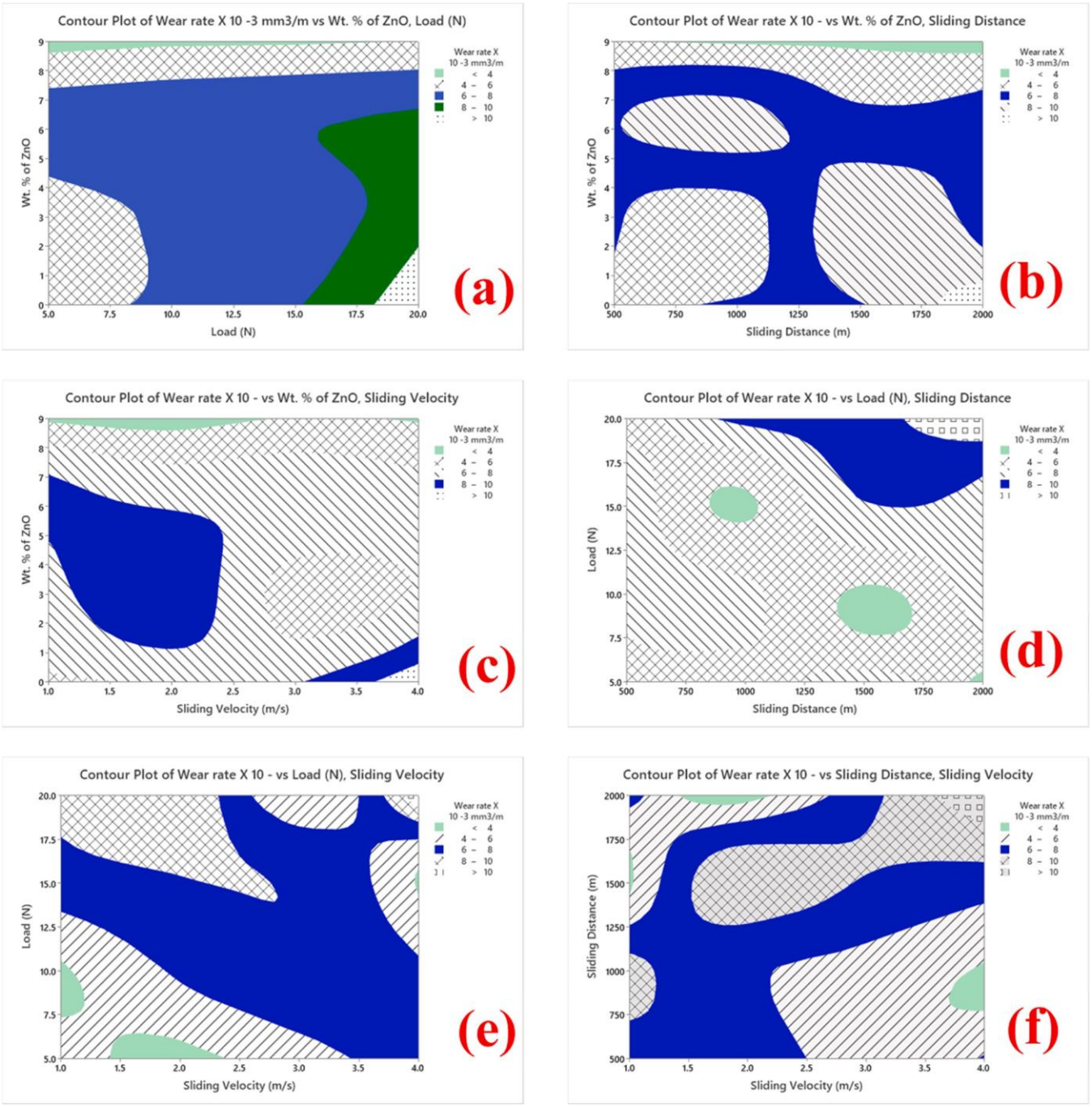

Fig. 15. Contour plots for W*R* obtained from the Taguchi analysis for various input parameters.

ZnO, P *versus* D and wt% of ZnO *versus* D. The COF of the composite samples increased with the applied load, when it was subjected to the accelerate wear tests. According to the aforementioned factors, the proposed materials possessed higher wear resistance, due to their hardness and increased ZnO content. The W*R* increased with the slide velocity. A high sliding velocity V(m/s) resulted to a deformation. This can be attributed to the rapid removal of material, in addition to the matrix softening. Pins also lose material as a result of formation of layer on their surface layers, which peeled off as time passed. Reinforced alloy possessed a higher W*R* than the composites. Composites have a lower W*R*, because they contained large Mg-3Al-ZnO particles that served as hardeners and self-lubricants. Increased hardness improved both wear and seizure resistance properties of compounds, as similarly reported [23,24].

3.2.3. *Interaction plot analysis*

The Figs. 17 and 18 show the interaction plots for W*R* and COF, respectively. The improved wear resistance of Mg-3Al-ZnO can be traced to its ability to smooth and blunt the protrusions of the reinforcements during sliding. A layer of self-lubricating particles was formed when the sliding distance was increased, reducing wear. W*R* increased as the sliding distance increased for alloys with reinforced plates. The eventually pin failed, because it became weak when the contact surface was too hot, resulting to more

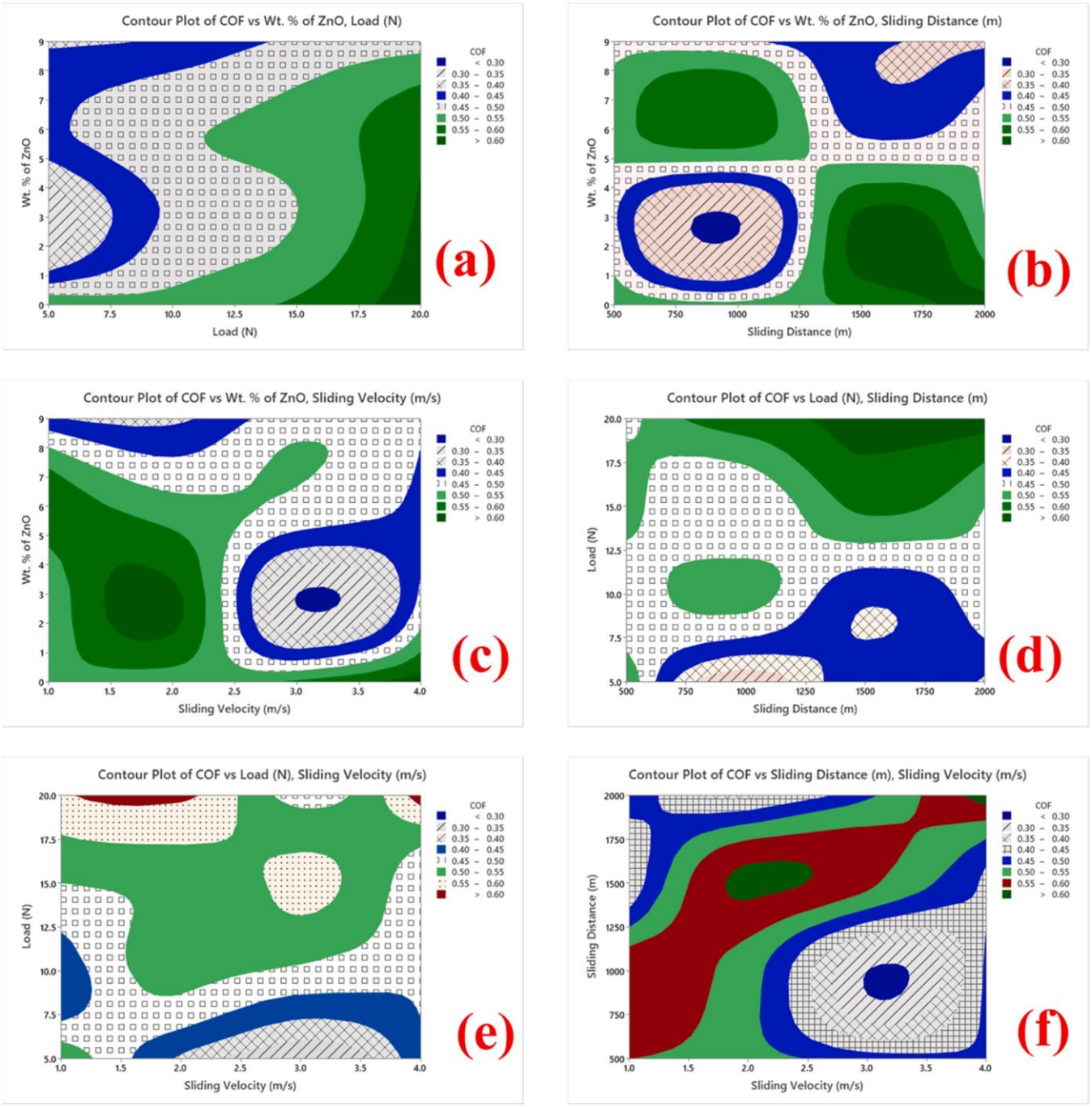

Fig. 16. Contour plots for COF obtained from the Taguchi analysis for various input parameters.

material loss. Composites were more efficient at longer distances than reinforced alloys, due to their lower hardness. The ZnO layer also exhibited benefit of reducing the W*R* of the composite matrix by serving as an insulating layer between the in-contact surfaces [21,24–26].

3.2.4. *ANOVA*

Using ANOVA, the distribution of W*R* and COF parameters, such as wt% of ZnO, P, V and D were studied for Mg-3Al-ZnO composites. Table 7 presents ANOVA for W*R*. According to the F-value, the reinforcement and sliding distance accounted for the majority of the factors, while the P factor determined others. ANOVA for COF is presented in Table 8. It was evident that V recorded the greatest impact, followed by ZnO content, D and P [17], as presented in Table 8. Eqs. (3) and (4) later show the regression equation for W*R* and COF, respectively.

3.2.5. *Regression analysis*

The important factors were used to create equations that could estimate the W*R* and COF of the composite samples, using

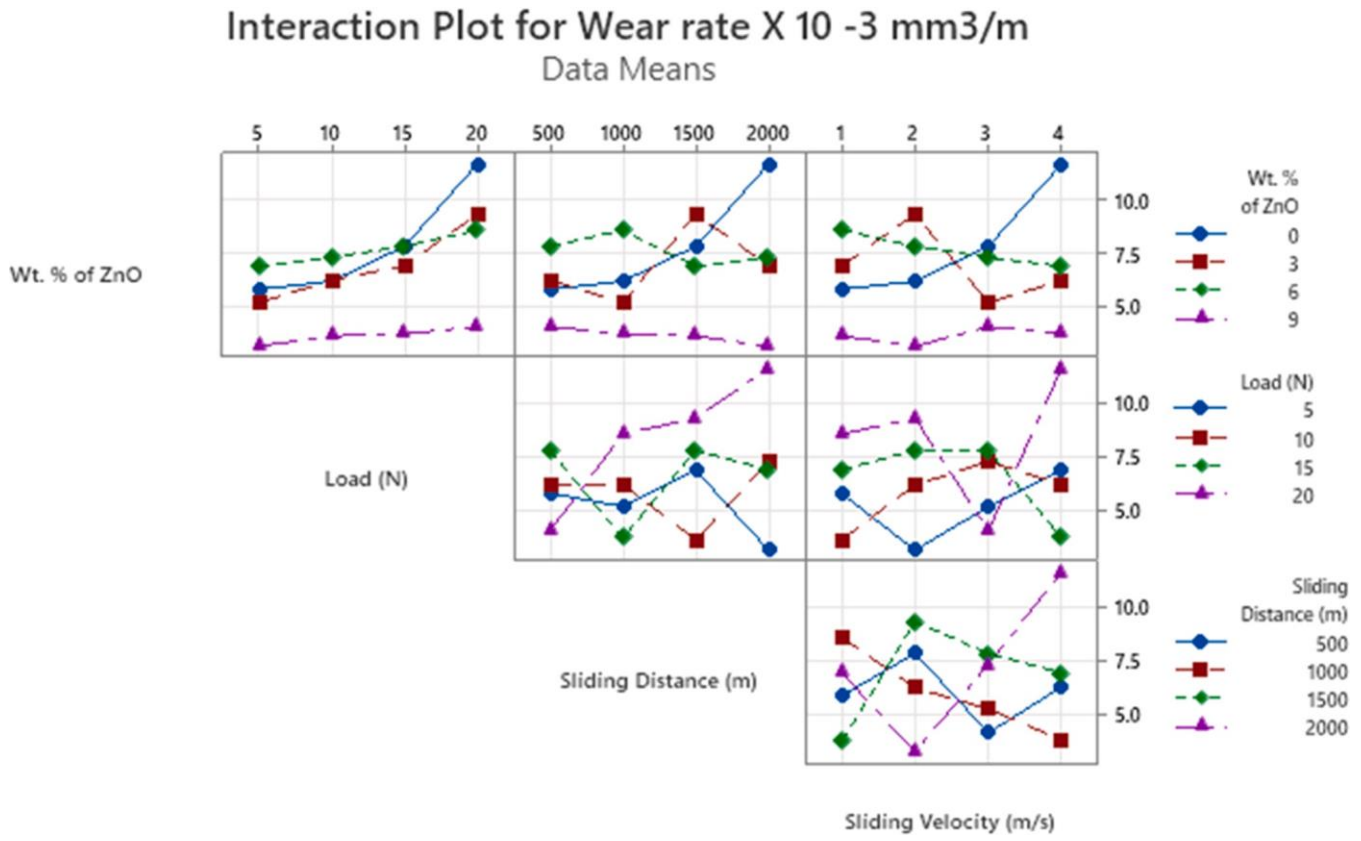

Fig. 17. Interaction plots of W*R* obtained for the input parameters wt% of ZnO, L, D and V.

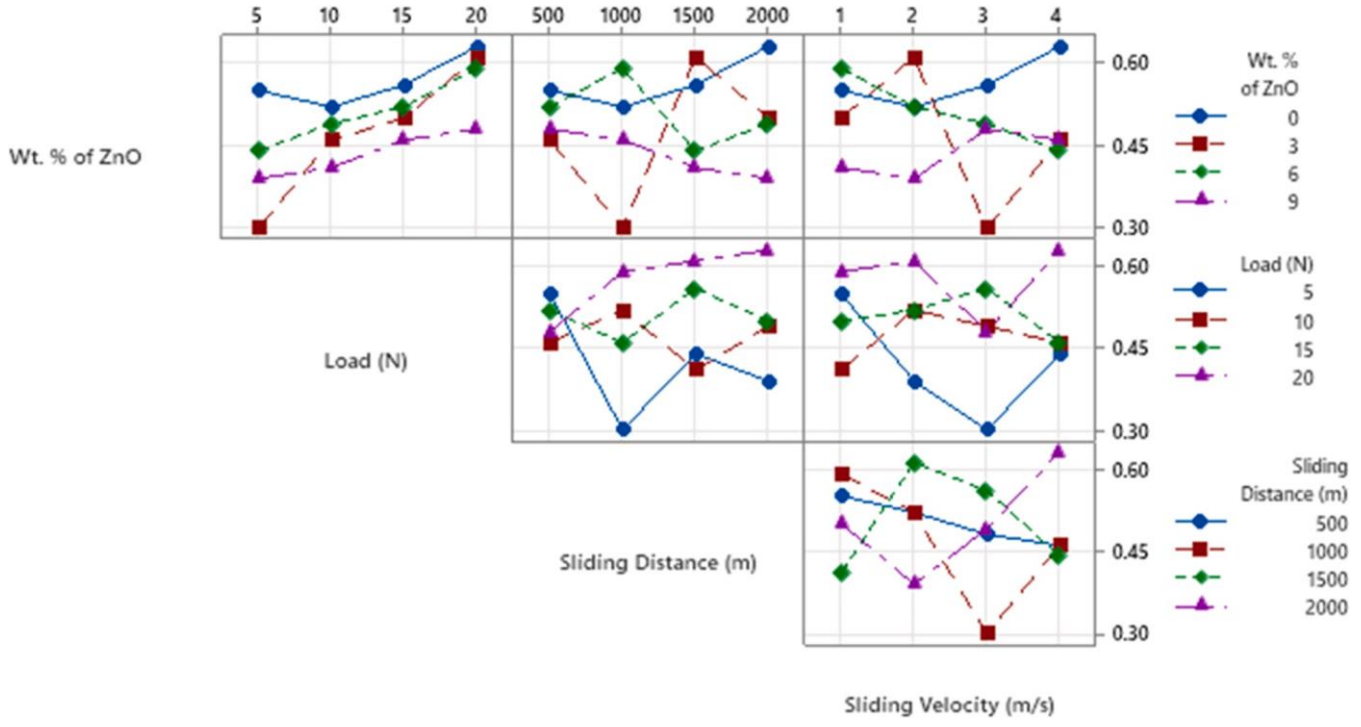

Fig. 18. Interaction plots of COF obtained for the input parameters wt% of ZnO, L, D and V.

Table 7
ANOVA for W*R*.

Source	DF	Adj SS	Adj MS	F-value	P-value
wt% ZnO	3	45.744	15.2479	20.08	0.017
P (N)	3	22.332	7.4441	9.80	0.046
V (m/s)	3	5.337	1.7789	2.34	0.251
D (m)	3	2.543	0.8477	1.12	0.465
Error	3	2.278	0.7592		
Total	15	78.234			

Table 8
ANOVA for COF.

Source	DF	Adj SS	Adj MS	F-value	P-value
wt% ZnO	3	0.037919	0.012640	4.56	0.122
P(N)	3	0.053119	0.017706	6.39	0.081
V (m/s)	3	0.003869	0.001290	0.47	0.727
D (m)	3	0.007769	0.002590	0.93	0.522
Error	3	0.008319	0.002773		
Total	15	0.110994			

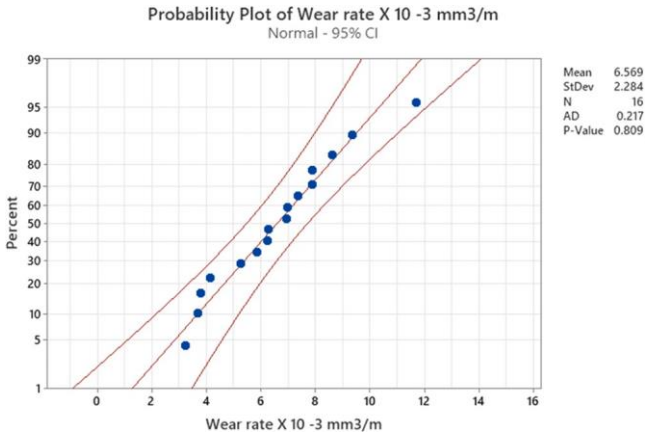

Fig. 19. Probability plot of W*R*.

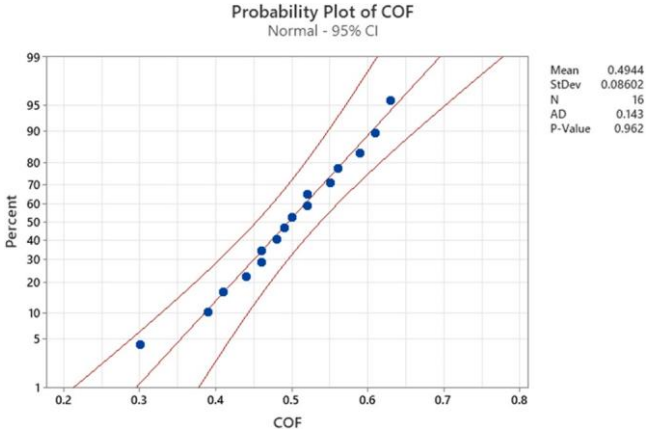

Fig. 20. Probability plot of COF.

the regression analysis. Therefore, regression Eqs. (4) and (5) were developed specifically to select parameters and determine the optimal output variables. Figs. 19 and 20 show the probability plots of W*R* and COF. Both Figs evidently depict that all the errors were within the limit by analysing for 95% of confidence intervals.

Regression equation for WR

$$\mathrm{WR}\ X10^{-3}\left(\frac{mm^3}{m}\right) = 6.569 + 1.348A_1 + 0.391A_2 + 1.124A_3 - 2.864A_4 - 1.255B_1 - 0.678B_2 + 0.049B_3 + 1.883B_4 - 0.535C_1 - 0.594C_2 + 0.394C_3 + 0.735C_4 - 0.285D_1 + 0.104D_2 - 0.423D_3 + 0.604D_4 \quad (4)$$

Regression equation for COF

$$\mathrm{COF} = 0.4944 + 0.0706A_1 - 0.0269A_2 + 0.0156A_3 - 0.0594A_4 - 0.0744B_1 - 0.0244B_2 + 0.0156B_3 + 0.0831B_4 + 0.0081C_1 - 0.0269C_2 + 0.0106C_3 + 0.0081C_4 + +0.0181D_1 + 0.0156D_2 - 0.0369D_3 + 0.0031D_4 \quad (5)$$

3.2.6. *Worn surface analysis*

Considering the worn surface of Mg-3Al-ZnO composites shown in Fig. 2(a)-(f), Fig. 2(a) and (b) depict the worn surface of the composite with 3 wt% of ZnO particle. It further shows the bluntly impaired regions, blister wear and huge flow of material with a lateral shift, caused by heavy plastic deformation. Fig. 2(c) and (d) show the worn surface of the Mg-3 wt%Al-6 wt%ZnO composites. They also show the formation of small cavities and cracks on the surface of the wear track, which suggested dry sliding wear. On this surface, it can be further observed that rigid and hollow formed much more shallowly in the composites than they did in unreinforced alloys. This was resulted to the presence of reinforcing particles in the matrix materials. However, there was wear debris that accumulated on the wear track. This indicated that the wear occurred due to the presence of ZnO particles in the composites. The deformed plastic shrinkage was reduced significantly, because of the presence of ZnO particles. The ZnO particles acted as a barrier to displacements and thereby increased the wear resistance. When ZnO increased, both W*R* and COF decreased.

Additionally, Fig. 2(e) and (f) show the worn surface images of the Mg-3 wt%Al-9 wt%ZnO composites. From the images, it was significantly observed that the ZnO particles contribution was high, because the sample contained 9 wt. of ZnO particles. The wear track was also observed significantly from the SEM images. The distribution of the ZnO particles was uniform on the worn samples. It was observed that the composite samples experienced abrasive wear. This can be attributed to more wt% of the ZnO particles presence in the matrix. All these occurrences contributed to the improved wear resistance of the ZnO reinforced Mg-based composites. Fig. 2(a-d) depict the adhesion type of wear for all the specimen prepared, using PM method. Unreinforced magnesium alloy showed the plough mechanism confirmed by severe ploughing of material, due to the absence of hard reinforcement. The worn marks were visible in all directions. The inclusion of ZnO in Mg matrix decreased the removal of matrix material, as observed in Fig. 2(b-d). The same phenomenon of low wear rate was observed on C/ZrO_2 composites at higher sliding velocity, as reported by Jha et al. [50] and Zhu et al. [51].

4. Conclusions

ZnO reinforced with Mg-3 wt%Al composites were fabricated, using PM technique and their microstructures and properties were studied. From the results obtained, the following concluding remarks can be deduced:

- SEM analysis of Mg-3Al-ZnO composite powder showed that the ZnO particles distributed uniformly within the matrix. This can be attributed to the correct choice of a suitable milling process. Similarly, the SEM image of Mg-3Al-ZnO sintered composites established proper distribution of ZnO within the matrix formed by Mg-3 wt%Al.
- XRD analysis established the presence of Mg-3Al matrix and ZnO peak in ball milled and sintered composite samples, and confirmed that the composites had no intermetallic phases.
- The experimental density and porosity of the sintered Mg-3 wt %Al, Mg-3 wt%Al-3 wt%ZnO, Mg-3 wt%Al-6 wt%ZnO and Mg-3 wt %Al-9 wt%ZnO composites were examined. It was evident that addition of reinforcements increased the density of the composites.
- The addition of 3–9 wt% of ZnO to the matrix of Mg-3Al increased the hardness of the composites. Comparatively, Mg-3 wt%Al-9 wt %ZnO composite samples recorded the highest compressive strength, among the Mg-3Al alloy samples. Therefore, both compressive strength and hardness increased with an increase in inclusion of ZnO in Mg matrix at the expense of its ductility; ductility reduced. Therefore, all its mechanical properties were not improved. However, both compressive strength and hardness are important properties in engineering and biomedical applications, especially where they are specifically and inevitably required.
- Corrosion resistance and wear behaviors of the composite samples were good, due to ZnO addition when compared with unreinforced alloy samples. Evidently, the corrosion resistance increased with an increase in ZnO, as validated with the SEM image of corroded sample. Therefore, for biomedical implant, the corrosion resistance of the implant material is a significant factor to be considered before selection of implants. Magnesium matrix composite is also suitable for biomedical applications.
- Abrasive wear was recorded on the samples with a high weight percentage of ZnO in the matrix, as observed from the SEM worn surface analysis.
- From the ANOVA analysis, it was evident that ZnO content was a highly significant factor that influenced the wear rate, while load mostly influenced COF of the composite samples during wear testing. The same results were evident from the S/N ratio analysis.

Finally, Mg-3Al-9 wt%ZnO matrix composite is an ideal material for industrial applications. It is suitable for other numerous real-world utilizations, considering the current increasing use of structural materials with enhanced wear resistance. Mg-3Al-9 wt%ZnO is an exceptional discontinuous reinforcement with outstanding CS, hardness and low density. Importantly, Mg-3Al-9 wt%ZnO composite has a potential of overcoming the cost obstacle for unlimited application in automotive parts and medical devices.

CRediT authorship contribution statement

Conceived and designed the experiments; S. Jayasathyakawin, M. Ravichandran, Sikiru Oluwarotimi Ismail, G.Veerappan. Performed the experiments; S. Jayasathyakawin, M. Ravichandran, Sikiru analyzed and interpreted the data; S. Jayasathyakawin, M. Ravichandran, Sikiru Oluwarotimi Ismail, G.Veerappan contributed reagents, materials, analysis tools or data; S. Jayasathyakawin, M. Ravichandran wrote the paper: S. Jayasathyakawin, M. Ravichandran, Sikiru Oluwarotimi Ismail, G.Veerappan

Data Availability

No data was used for the research described in the article.

Declaration of Competing Interest

The authors declare that they have no known competing financial interests or personal relationships that could have appeared to influence the work reported in this paper.

References

[1] W. Yu, X. Li, M. Vallet, L. Tian, High temperature damping behavior and dynamic Young's modulus of magnesium matrix composite reinforced by Ti_2AlC MAX phase particles, Mech. Mater. 129 (2019) 246–253, https://doi.org/10.1016/j.mechmat.2018.12.001

[2] T. Thirugnanasambandham, J. Chandradass, P.B. Sethupathi, M.L.J. Martin, Experimental study of wear characteristics of Al_2O_3 reinforced magnesium based metal matrix composites, Mater. Today Proc. 4 (2019) 211–218, https://doi.org/10.1016/j.matpr.2019.04.140

[3] J. Hou, W. Du, C. Zhao, X. Du, Z. Wang, S. Li, K. Liu, Study on the behaviors of multi-walled carbon nanotubes modified by gemini sulfonate dispersant and their reinforced magnesium matrix, Mater. Chem. Phys. 229 (2019) 279–285, https://doi.org/10.1016/j.matchemphys.2019.03.028

[4] C. Xie, H. Li, X. Zhou, C. Sun, Corrosion behavior of cold sprayed pure zinc coating on magnesium, Surf. Coat. Technol. 374 (2019) 797–806, https://doi.org/10.1016/j.surfcoat.2019.06.068

[5] F. Witte, N. Hort, C. Vogt, S. Cohen, K.U. Kainer, R. Willumeit, F. Feyerabend, Degradable biomaterials based on magnesium corrosion, C. Opin. Solid State Mater. Sci. 12 (2008) 63–72, https://doi.org/10.1016/j.cossms.2009.04.001

[6] H. Yong, R. Li, Effect of particulate reinforcement on wear behavior of magnesium matrix composites, Trans. Nonferrous Met. Soc. China 22 (2012) 2659–2664, https://doi.org/10.1016/S1003-6326(11)61514-8

[7] J. Capek, D. Vojtech, Effect of sintering conditions on the microstructural and mechanical characteristics of porous magnesium materials prepared by powder metallurgy, Mater. Sci. Eng. C. 43 (2014) 494–501, https://doi.org/10.1016/j.msec.2013.10.014

[8] M.E. Turan, Y. Sun, F. Aydin, H. Zengin, Y. Turen, H. Ahlatci, Effects of carbonaceous reinforcements on microstructure and corrosion properties of magnesium matrix composites, Mater. Chem. Phys. 218 (2018) 182–188, https://doi.org/10.1016/j.matchemphys.2018.07.050

[9] V.K. Bommala, M.G. Krishna, C.T. Rao, Magnesium matrix composites for biomedical applications: a review, 72-29, J. Magnes. Alloy 7 (2019), https://doi.org/10.1016/j.jma.2018.11.001

[10] K.B. Nie, K. Wu, X.J. Wang, K.K. Deng, Y.W. Wu, M.Y. Zheng, Multidirectional forging of magnesium matrix composites: effect on microstructures and tensile properties, Mater. Sci. Eng. A 527 (2010) 7364–7368, https://doi.org/10.1016/j.msea.2010.08.007

[11] A. Vahid, P. Hodgson, Y. Li, Reinforced magnesium composites by metallic particles for biomedical applications, Mater. Sci. Eng. A. 685 (2017) 349–357, https://doi.org/10.1016/j.msea.2017.01.017

[12] Y.L. Xi, D.L. Chai, W.X. Zhang, J.E. Zhou, Titanium alloy reinforced magnesium matrix composite with improved mechanical properties, Scr. Mater. 54 (2006) 19–23, https://doi.org/10.1016/j.scriptamat.2005.09.020

[13] P. Bansal, G. Singh, H.S. Sidhu, Investigation of surface properties and corrosion behavior of plasma sprayed HA/ZnO coatings prepared on AZ31 Mg alloy, Surf. Coat. Technol. 401 (2020) 126241, https://doi.org/10.1016/j.surfcoat.2020.126241

[14] R. Guan, A.F. Cipriano, Z. Zhao, J. Lock, D. Tie, T. Zhao, T. Cui, H. Liu, Development and evaluation of a magnesium–zinc–strontium alloy for biomedical applications — alloy processing, microstructure, mechanical properties, and biodegradation, Mater. Sci. Eng. C. 33 (2013) 3661–3669, https://doi.org/10.1016/j.msec.2013.04.054

[15] B. Selvam, P. Marimuthu, R. Narayanasamy, V. Anandakrishnan, K.S. Tun, M. Gupta, M. Kamaraj, Dry sliding wear behaviour of zinc oxide reinforced magnesium matrix nano-composites, Mater. Des. 58 (2014) 475–481, https://doi.org/10.1016/j.matdes.2014.02.006

[16] R. Kumar, R. Singh, M. Singh, P. Kumar, On ZnO nano particle reinforced PVDF composite materials for 3D printing of biomedical sensors, J. Manuf. Process 60 (2020) 268–282, https://doi.org/10.1016/j.jmapro.2020.10.027

[17] F. Chen, B. Tang, P. Jin, L. Zhang, W. Fei, Tensile properties and hot extrusion behavior of ZnO-coated Mg2B2O5w/6061 Al composites, Trans. Nonferrous Met. Soc. China 25 (2015) 412–419, https://doi.org/10.1016/S1003-6326(15)63618-4

[18] M. Carboneras, L.S. Hernandez, J.A. Del Valle, M.C. García-Alonso, M.L. Escudero, Corrosion protection of different environmentally friendly coatings on powder metallurgy magnesium, J. Alloy. Compd. 496 (1–2) (2010) 442–448, https://doi.org/10.1016/j.jallcom.2010.02.043

[19] S.B. Bhosale, S. Bhowmik, A. Ray, Multi criteria decision making for selection of material composition for powder metallurgy process, Mater. Today Proc. 5 (2018) 4615–4620, https://doi.org/10.1016/j.matpr.2017.12.032

[20] S. Raynova, F. Yang, L. Bolzoni, Mechanical behaviour of induction sintered blended elemental powder metallurgy Ti alloys, Mater. Sci. Eng. A. 799 (2021) 140157, https://doi.org/10.1016/j.msea.2020.140157

[21] S.V. Alagarsamy, M. Ravichandran, Investigations on tribological behaviour of AA7075-TiO2 composites under dry sliding conditions, Ind. Lubr. Tribol. 71 (9) (2019) 1064–1071, https://doi.org/10.1108/ILT-01-2019-0003

[22] S. Dharmalingam, R. Subramanian, M. Kok, Optimization of abrasive wear performance in aluminium hybrid metal matrix composites using taguchi-grey

relational analysis, Proc. Inst. Mech. Eng. J: J. Eng. Tribol. 227 (7) (2013) 749–760. https://doi.org/10.1177/1350650112467947.
[23] B. Ashok Kumar, N. Murugan, Metallurgical and mechanical characterization of stir cast AA6061-T6–AlNp composite, Mater. Des. 40 (2012) 52–58, https://doi.org/10.1016/j.matdes.2012.03.038
[24] N. Radhika, R. Raghu, Dry sliding wear behaviour of aluminium Al–Si12Cu/TiB2 metal matrix composite using response surface methodology, Tribol. Lett. 59 (2) (2015) 1–9, https://doi.org/10.1007/s11249-015-0516-3
[25] N. Radhika, R. Raghu, Evaluation of dry sliding wear characteristics of LM 13 Al/B4C composites, Tribol. Ind. 37 (1) (2015) 20–28.
[26] N. Radhika, R. Raghu, Prediction of mechanical properties and modeling on sliding wear behavior of LM25/TiC composite using response surface methodology, Part. Sci. Technol. 36 (1) (2018) 104–111, https://doi.org/10.1080/02726351.2016.1223773
[27] A. Kumar, S. Kumar, N.K. Mukhopadhyay, Introduction to magnesium alloy processing technology and development of low-cost stir casting process for magnesium alloy and its composites, J. Magnes. Alloy 6 (3) (2018) 245–254, https://doi.org/10.1016/j.jma.2018.05.006
[28] M.A.El Baradie, Manufacturing aspects of metal matrix composites, J. Mater. Process. Technol. 24 (1) (1990) 261–272, https://doi.org/10.1016/0924-0136(90)90187-Y
[29] H. Zhou, L. Hu, Y. Sun, H. Zhang, C. Duan, H. Yu, Synthesis of nanocrystalline AZ31 magnesium alloy with titanium addition by mechanical milling, Mater. Charact. 113 (2016) 108–116, https://doi.org/10.1016/j.matchar.2016.01.014
[30] G. Mahajan, N. Karve, U. Patil, P. Kuppan, K. Venkatesan, Analysis of microstructure, hardness and wear of Al-SiC-TiB2 hybrid metal matrix composite, Indian J. Sci. Technol. 8 (2015) 101–105, https://doi.org/10.17485/ijst/2015/v8iS2/59081
[31] G.E.J. Poinern, S. Brundavanam, D. Fawcett, Biomedical magnesium alloys: a review of material properties, surface modifications and potential as a biodegradable orthopaedic implant, Am. J. Biomed. Eng. 6 (2012) 218–240, https://doi.org/10.5923/j.ajbe.20120206.02
[32] A. Abbas, S. Huang, ECAP effects on microstructure and mechanical behavior of annealed WS2/AZ91 metal matrix composite, J. Alloy. Compd. 835 (2020) 155466, https://doi.org/10.1016/j.jallcom.2020.155466
[33] X.N. Gu, S.S. Li, X.M. Li, Y.B. Fan, Magnesium based degradable biomaterials: a review, Front. Mater. Sci. 8 (2014) 200–218, https://doi.org/10.1007/s11706-014-0253-9
[34] R. Kumar, Dr.C.N. Chandrappa, Synthesis and characterization of Al-SiC functionally graded material composites using powder metallurgy techniques, Int. J. Innov. Res. Technol. Sci. Eng. 3 (2014) 15464–15471, https://doi.org/10.15680/IJIRSET.2014.0308054
[35] N. Saha, K. Keskinbora, E. Suvaci, Sintering, microstructure, mechanical, and antimicrobial properties of HAp-ZnO biocomposites, J. Biomed. Mater. Res. Part B: Appl. Biomater. 95 (2010) 430–440, https://doi.org/10.1002/jbm.b.31734
[36] A.K. Chaubey, S. Scudino, M. Samadi Khoshkhoo, K.G. Prashanth, N.K. Mukhopadhyay, B.K. Mishra, J. Eckert, High-strength ultrafine grain Mg-7.4%Al alloy synthesized by consolidation of mechanically alloyed powders, J. Alloy. Compd. 610 (2014) 456–461, https://doi.org/10.1016/j.jallcom.2014.05.029
[37] A.K. Chaubey, S. Scudino, M. Samadi Khoshkhoo, K.G. Prashanth, N.K. Mukhopadhyay, B.K. Mishra, J. Eckert, Synthesis and characterization of nanocrystalline Mg-7.4%Al powders produced by mechanical alloying, Metals 3 (2013) 58–68, https://doi.org/10.3390/met3010058
[38] Y. Shadangi, K. Chattopadhyay, N.K. Mukhopadhyay, Powder metallurgical processing of Al matrix composite reinforced with AlSiCrMnFeNiCu high-entropy alloys: Microstructure, thermal stability, and microhardness, J. Mater. Res 38 (2023) 248–264, https://doi.org/10.1557/s43578-022-00866-x
[39] Y. Nandini Singh, N.K. Shadangi, Mukhopadhyay, phase evolution and thermal stability of low-density MgAlSiCrFe high-entropy alloy processed through mechanical alloying, Trans. Indian Inst. 73 (2020) 2377–2386, https://doi.org/10.1007/s12666-020-02039-y
[40] Y. Shadangi, S. Sharma, V. Shivam, J. Basu, K. Chattopadhyay, B. Majumdar, N.K. Mukhopadhyay, Fabrication of Al–Cu–Fe quasicrystal reinforced 6082 aluminium matrix nanocomposites through mechanical milling and spark plasma sintering, J. Alloy. Compd. 828 (2020) 154258, https://doi.org/10.1016/j.jallcom.2020.154258
[41] A. Suguna, S. Prabhu, M. Selvaraj, M. Geerthana, A. Silambarasan, M. Navaneethan, R. Ramesh, C. Sridevi, Annealing effect on photocatalytic activity of ZnO nanostructures for organic dye degradation, J. Mater. Sci. Mater. Electron 33 (2022) 8868–8879, https://doi.org/10.1007/s10854-021-06942-y
[42] S. Prabhu, M. Pudukudy, S. Sohila, S. Harish, M. Navaneethan, D. Navaneethan, R. Ramesh, Y. Hayakawa, Synthesis, structural and optical properties of ZnO spindle/reduced graphene oxide composites with enhanced photocatalytic activity under visible light irradiation, Opt. Mater. 79 (2018) 186–195, https://doi.org/10.1016/j.optmat.2018.02.061
[43] S. Prabhu, S. Megala, S. Harish, M. Navaneethan, P. Maadeswaran, S. Sohila, R. Ramesh, Enhanced photocatalytic activities of ZnO dumbbell/reduced graphene oxide nanocomposites for degradation of organic pollutants via efficient charge separation pathway, Appl. Surf. Sci. 487 (2019) 1279–1288, https://doi.org/10.1016/j.apsusc.2019.05.086
[44] S. Prabhu, M. Pudukudy, S. Harish, M. Navaneethan, S. Sohila, K. Murugesan, R. Ramesh, Facile construction of djembe-like ZnO and its composite with g-C3N4 as a visible-light-driven heterojunction photocatalyst for the degradation of organic dyes, Mater. Sci. Semicond. 106 (2020) 104754, https://doi.org/10.1016/j.mssp.2019.104754
[45] C. Jayakrishnan, S.R. Sheeja, J. Duraimurugan, S. Prabhu, R. Ramesh, G. Suresh Kumar, K.G. Subhash, Mohd Shkir, M.R. Pallavolu, Synthesis of dumbbell-shaped ZnO nanostructures for energy storage and photocatalytic dye degradation applications, Mater. Technol. 37 (14) (2022) 3006–3016, https://doi.org/10.1080/10667857.2022.2107821
[46] M. Satheesh, M. Pugazhvadivu, Investigation on physical and mechanical properties of Al6061-silicon carbide (SiC)/Coconut shell ash (CSA) hybrid composites, Phys. B Condens Matter 572 (2019) 70–75, https://doi.org/10.1016/j.physb.2019.07.058
[47] S. Jayasathyakawin, M. Ravichandran, Experimental Investigations on effect of silicon carbide on microstructure and mechanical properties in Mg-3 wt% Al alloy matrix using powder metallurgy, Silicon 14 (2022) 9163–9173, https://doi.org/10.1007/s12633-022-01834-0
[48] L. Azaath, Mamundi, Experimental investigations on the mechanical properties, microstructure and corrosion effect of Cu-20Al-4Ni/SiC composites synthesized using powder metallurgy route, Silicon 14 (11) (2022) 5993–6002, https://doi.org/10.1007/s12633-021-01363-2
[49] K.S. Tun, M. Gupta, Improving mechanical properties of magnesium using nano-yttria reinforcement and microwave assisted powder metallurgy method', Compos Sci. Technol. 67 (13) (2007) 2657–2664, https://doi.org/10.1016/j.compscitech.2007.03.006
[50] N. Jha, A. Badkul, D.P. Mondal, S. Das, M. Singh, Sliding wear behaviour of aluminum syntactic foam: a comparison with Al–10 wt% SiC composites, Tribol. Int 44 (2011) 220–231, https://doi.org/10.1016/j.triboint.2010.10.004
[51] H.G. Zhu, Y.L. Ai, J. Min, Q. Wu, H.Z. Wang, Dry sliding wear behavior of Al-based composites fabricated by exothermic dispersion reaction in an Al–ZrO2–C system, Wear 268 (2010) 1465–1471, https://doi.org/10.1016/j.wear.2010.02.023
[52] G. Veerappan, M. Ravichandran, M. Meignanamoorthy, V. Mohanavel, Characterization and properties of silicon carbide reinforced Ni-10Co-5Cr (Superalloy) matrix composite produced via powder metallurgy route, Silicon 13 (4) (2021) 973–984, https://doi.org/10.1007/s12633-020-00455-9
[53] D.M. Jarząbek, The impact of weak interfacial bonding strength on mechanical properties of metal matrix – ceramic reinforced composites, Compos. Struct. 201 (2018) 352–362, https://doi.org/10.1016/j.compstruct.2018.06.071
[54] M. Satheesh, M. Pugazhvadivu, Investigation on physical and mechanical properties of Al6061-silicon carbide (SiC)/coconut shell ash (CSA) hybrid composites, Phys. B Condens. 572 (2019) 70–75, https://doi.org/10.1016/j.physb.2019.07.058